https://doi.org/10.5194/egusphere-2023-2485
Preprint. Discussion started: 13 November 2023


# Sourcing and Long-Range Transport of Particulate Organic Matter in River Bedload: Rio Bermejo, Argentina

Sophia Dosch[1,2], Niels Hovius[1,2], Marisa Repasch[3], Joel Scheingross[4], Jens M. Turowski[1], Stefanie Tofelde[5], Oliver Rach[1], Dirk Sachse[1,6]

[1]GFZ German Research Centre for Geosciences, Potsdam, Germany
[2]Universität Potsdam, Institute of Geosciences, Potsdam, Germany
[3]University of Colorado Boulder, Institute of Arctic and Alpine Research, Boulder, CO, USA
[4]University of Nevada Reno, Department of Geological Sciences and Engineering, Nevada Geosciences, Reno, NV, USA
[5]Freie Universität Berlin, Institute of Geological Sciences, Berlin, Germany
[6]Humboldt Universität zu Berlin, Department of Geography, Berlin, Germany

*Correspondence to*: Sophia Dosch (sophia.dosch@gfz-potsdam.de)

https://doi.org/10.5194/egusphere-2023-2485
Preprint. Discussion started: 13 November 2023


**Abstract**. Fluvial transport of organic carbon from the terrestrial biosphere to the oceans is an important term in the global carbon cycle. Traditionally, the long-term burial flux of fluvial particulate organic carbon (POC) is estimated using river suspended sediment flux; however, organic carbon can also travel in river bedload as coarse particulate organic matter ($POM_{Bed}$). Estimates of fluvial POC export to the ocean are highly uncertain because few studies document $POM_{bed}$ sources, flux and evolution during long-range fluvial transport from uplands to ocean basins. This knowledge gap limits our ability to determine the global terrestrial organic carbon burial flux. In this study we investigate the flux, sources and transformations of $POM_{Bed}$ during fluvial transport over a ~1300 km long reach of the Rio Bermejo, Argentina, which has no tributary inputs. To constrain sourcing of $POM_{Bed}$, we analysed the composition and stable hydrogen and carbon isotope ratios ($\delta^2H$, $\delta^{13}C$) of plant wax biomarkers from $POM_{Bed}$ at six locations along the Rio Bermejo, and compared this to samples of suspended sediment, soil, leaf litter and floating organic debris ($POM_{float}$) from both the lowland and headwater river system. Across all samples, we found no discernible differences in *n*-alkane average chain length or $nC_{29}$ $\delta^{13}C$ values, indicating a common origin for all sampled $POM_{Bed}$. Leaf litter and $POM_{float}$ $nC_{29}$ $\delta^2H$ values decrease with elevation, making it a useful proxy for $POM_{Bed}$ source elevation. Biomarker $\delta^2H$ values suggest that $POM_{Bed}$ is a mix of distally-derived headwater and locally-recruited floodplain sources at all sampling locations. These results indicate that $POM_{Bed}$ can be preserved during transport through lowland rivers for hundreds of kilometres. However, the $POM_{Bed}$ flux decreases with increasing transport distance, suggesting mechanical comminution of these coarse organic particles, and progressive transfer into the suspended load. Our provisional estimates suggest that the carbon flux from $POM_{Bed}$ comprises less than 1 percent of the suspended load POC flux in the Rio Bermejo. While this represents a small portion of the river POC flux, this coarse and high density material likely has a higher probability of deposition and burial in sedimentary basins, potentially allowing it to be more effective in long-term $CO_2$ drawdown relative to fine suspended particles. Because the rate and ratio of $POM_{Bed}$ transport versus comminution likely varies across tectonic and climatic settings, additional research is needed to determine the importance of $POM_{Bed}$ in the global carbon cycle.

https://doi.org/10.5194/egusphere-2023-2485
Preprint. Discussion started: 13 November 2023


## 1 Introduction

The burial of organic carbon (OC) in soils and sedimentary depocenters can remove carbon from the atmosphere over timescales of centuries to millennia (Hilton and West, 2020; Galy et al., 2015; Blair and Aller, 2012; Battin et al., 2009; Hayes et al., 1999; Stallard, 1998; France-Lanord and Derry, 1997; Berner, 1982). OC buried in sedimentary basins is mainly sourced from tectonically active environments, like mountainous areas where physical erosion mobilizes hillslope bedrock and soil, generating sediment (e.g., Galy et al., 2015; Blair and Aller, 2012; Stallard, 1998). Rivers play a key role as conduits in the carbon cycle, moving OC eroded from rock, soil and vegetation from the terrestrial to marine carbon reservoir if the transported carbon is buried in a sedimentary basin (e.g., Schlünz and Schneider, 2000). The long spatial and temporal scales of this transport allow for carbon transformation during transfer and intermittent storage (Blattmann et al., 2019; Galy et al., 2008), for instance in floodplains, estuaries, and coastal mud belts (Repasch et al., 2022; Scheingross et al., 2021; Canuel and Hardison, 2016; Aller, 1998).

It is usually assumed that once particulate organic matter (POM) from terrestrial sources has been transferred into rivers, it is transported with the fine suspended sediment (Kao et al., 2014). Estimates of POM flux, as opposed to dissolved OM, suggest that rivers deliver 110 – 230 MtC into the oceans annually (Galy et al., 2015). River bedload can comprise lithic fragments that contain fossil organic carbon (Smith et al., 2013b; Hage et al., 2020; Kao et al., 2014), a phase of particulate OC that might be oxidized and emit $CO_2$ during floodplain transit (Dellinger, 2023). However, a second organic bedload component exists – plant debris.

Particulate OM includes coarse plant material and can be abundant, ranging from 10 up to 80% of the total fluvial OC flux (Seo et al., 2008; West et al., 2011; Kao et al., 2014; Turowski et al., 2016). Hillslope mass wasting, overland flow, and flooding of riparian zones can mobilize leaf litter and woody debris into the fluvial routing system (Turowski et al., 2016; West et al., 2011; Wohl et al., 2009). Coarse POM can float at the river surface, where it is visible and accountable (e.g., Ruiz-Villanueva et al., 2019; West et al., 2011; Wohl et al., 2009), or it can move along the river bed where it is more difficult to observe and measure (e.g., Turowski et al., 2013). The physical, chemical, and biological breakdown of woody debris (Seo et al., 2008) resting in the landscape allows the material to become waterlogged within days or weeks (Hoover et al., 2010). This can increase the density of organic debris above the critical value of 1.0 g $cm^{-3}$ so that it will sink to the river (Turowski et al., 2016; Turowski et al., 2013). There, it can be transported with the bedload (e.g., Schwab et al., 2022; Hage et al., 2020; Lee et al., 2019; Turowski et al., 2016; Liu et al., 2016), and has been observed to comprise up to 75% of all coarse POM (Turowski et al., 2016).

Several studies describe fresh, coarse terrestrial organic debris transported to delta plains (Allen et al., 1979) and offshore(West et al., 2011) by turbidity currents (Hage et al., 2020; Liu et al., 2013; Tyson and Follows, 2000). When capped by muddy siliciclastic sediments, terrestrially sourced, coarse POM is protected from fast degradation (Hage et al., 2020; Lee et al., 2019; McArthur et al., 2016; Sparkes et al., 2015), leading to preservation rates of up to 70% (Hage et al., 2022; Kao et al., 2014). Coarse woody debris and litter fragments have been described in aged deep marine fan deposits (Lee et al., 2019) and up to

https://doi.org/10.5194/egusphere-2023-2485
Preprint. Discussion started: 13 November 2023


12% of the mass in exhumed turbidites layers (Turowski et al., 2016; Tyson and Follows, 2000). Taken together, these observations suggest that transport of terrestrial POM in river bedload may be a relevant pathway in the global carbon cycle (Hage et al., 2020; Lee et al., 2019; Kao et al., 2014), both during source to sink transit and in depocenters.

However, organic debris at the river bed is difficult to observe and quantify due to logistical difficulties in sampling and highly variable transport rates (Turowski et al., 2013). The occurrence, recruitment, sources and fate of $POM_{Bed}$ during transport has only been addressed for a few headwater streams (Turowski et al., 2016; Turowski et al., 2013; Bunte et al., 2016; Iroumé et al., 2020; Fogel and Lininger, 2023), and even less for lowland systems (Hage et al., 2022; Schwab et al., 2022). The paucity of work on where $POM_{Bed}$ is recruited from, and how long it endures long-range fluvial transport after erosion, makes it difficult to build a mechanistic model to predict bedload OC fluxes and quantify their role in the terrestrial OC cycle.

In this study, we evaluate the role of organic bedload in the OC cycle of a large lowland river, the Rio Bermejo in northwest Argentina. This river is a major tributary to the Rio Paraguay, draining a section of the eastern central Andes across an 800 km wide foreland without overwhelming human intervention (Repasch, 2023). The lowland portion of the Rio Bermejo has no major tributaries or distributaries over a flow distance of almost 1300 km, ruling out sediment mixing complexities inherent to dendritic drainage networks. We address three questions designed to understand the role of $POM_{Bed}$ in the terrestrial carbon cycle: 1) Is POM transported with bedload in the lowland Rio Bermejo? 2) If so, what are the source areas and mechanisms for $POM_{Bed}$ recruitment? 3) Does $POM_{Bed}$ survive long-range transport without transformation through the Rio Bermejo? To answer these questions, we collected organic-rich material traveling at the river bed, analyzed the geochemical composition of the collected organic-rich material and tracked changes in the organic material composition with increasing distance downstream from the headwaters.

## 2 Study Area, Sampling Methods and Analyses

### 2.1 Study area

The Rio Bermejo, catchment area of 120,283 $km^2$, drains the northern-western Argentinian Andes before crossing the Gran Chaco alluvial plain and joining the Rio Paraguay (Fig. 1a). The Rio Bermejo headwaters extend to the eastern limit of the arid Puna Plateau, at an elevation of ~4 km. Headwater streams drain the high-altitude dry grasslands, ultimately merging to form the upper Rio Bermejo in the north and the Rio San Francisco (a major headwater tributary of the Rio Bermejo) in the south (Fig. 1). In the southern headwaters, mean annual rainfall is around 1000 mm $yr^{-1}$ and dense Yungas forests cover deeply weathered foothills. In the northern headwaters, the hinterland comprises the Eastern Cordillera and the Sub-Andean zone with highly variable rainfall up to 1400 mm $yr^{-1}$ and Yungas montane forest (Fig. 1c). Steep relief and intense precipitation in these northern headwaters result in high sediment yields to the Rio Bermejo.

At the Andean Mountain front, the upper Rio Bermejo and the Rio San Francisco merge to form the lowland Rio Bermejo, a sand bed river crossing the foreland basin. Just after the headwater confluence, the lowland Bermejo is a braided, with river width varying from 1-3 km. 175 km downstream of the confluence, the river transitions into a meandering channel, with

https://doi.org/10.5194/egusphere-2023-2485
Preprint. Discussion started: 13 November 2023


105 migration rates from 40-80 m $yr^{-1}$. The channel width narrows to 170 m in the most downstream parts, towards the confluence with the Rio Paraguay (Repasch, 2023; Repasch et al., 2020; Sambrook Smith et al., 2016). where our downstream transect samples were capture. River depths ranges between 4 to 10 meters at high flow with channel depth deepening downstream (Sambrook Smith et al., 2016). Grain size analyses show downstream fining (Repasch et al., 2020) from medium sand, on average 280 µm in the headwaters, to very fine sand to silty sand, on average 90 µm in the downstream part of the river
110 (Sambrook Smith et al., 2016; McGlue et al., 2016). The daily water discharge averages 432 $m^3$ $s^{-1}$, however, the wet season discharge of the austral summer accounts for ~75% of the annual flow, with daily discharges up to 2,000 $m^3$ $s^{-1}$ (Golombek et al., 2021; Sambrook Smith et al., 2016). The Rio Bermejo delivers ~80 Mt $yr^{-1}$ of sediment to the Rio Paraguay. Sediment input from the Andean headwaters at the Bermejo-San Francisco confluence is significantly higher, ~103 Mt $yr^{-1}$, suggesting net deposition during foreland transit (Repasch et al., 2020). The Rio San Francisco contributes ~14% to the total suspended

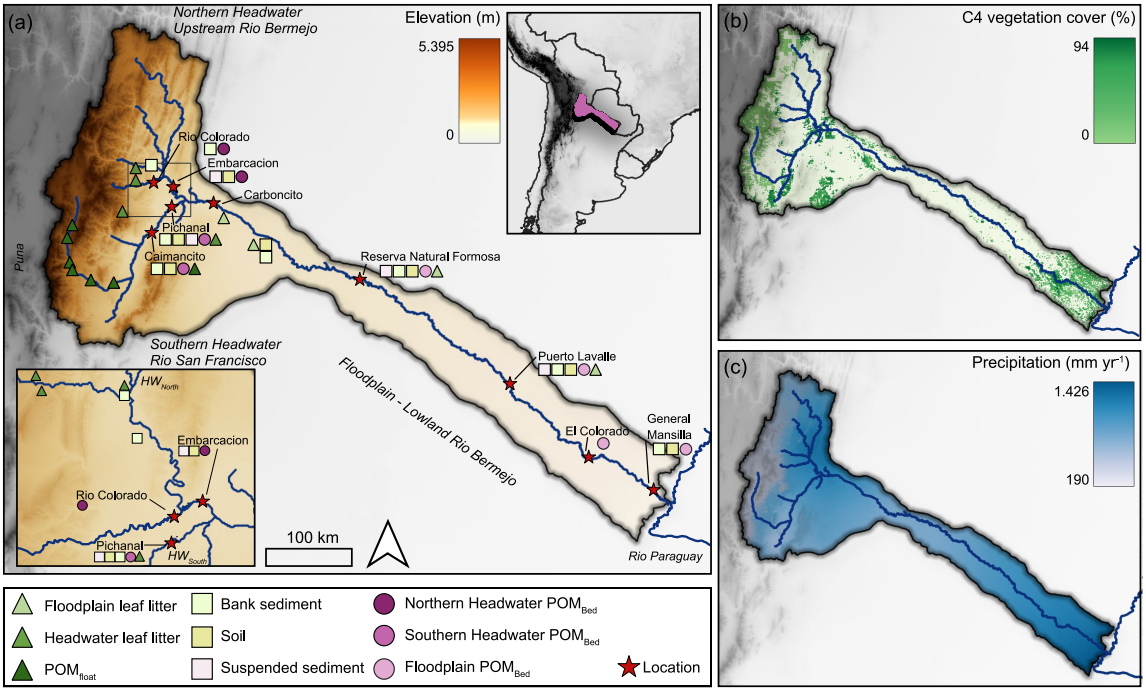


**Figure 1: Catchment overview of the Rio Bermejo mainstem and main headwater tributaries (a) Topographic map (ASTGTM, Spacesystems and Team, 2019) with sample types indicated at each sampling location. Top right: catchment location in Argentina. Bottom left: zoomed view of the tributary confluence at the mountain front. (b) C4 vegetation cover, as a percentage of total C3 and C4 vegetation cover (Powell et al., 2012). (c) Average annual precipitation rate (Hijmans et al., 2005).**

115 sediment load of the Rio Bermejo mainstem, whereas, the northern headwaters contribute ~86% (Repasch et al., 2020), likely reflecting the south to north gradient in precipitation, vegetation, and erosion rate.

Our work is focused on the Rio Bermejo downstream of the east Andean Mountain front, from the confluence of the Rio Bermejo-Rio San Francisco confluence (304 m. asl.) to the Rio Bermejo-Rio Paraguay confluence (50 m asl.). The linear

https://doi.org/10.5194/egusphere-2023-2485
Preprint. Discussion started: 13 November 2023


distance between these points is ~700 km, while the river has a channel length of ~1300 km due to its high sinuosity. Over this distance, no significant tributaries join the Rio Bermejo, making it an ideal setting for our source to sink study of organic bed material.

**Table 1: Overview of the bedload sampling sites, including location ID, location name, longitude, latitude, respective part of the Rio Bermejo catchment, linear downstream distance from the mountain front (tributary confluence), sampling year, and number (n) of all bedload samples collected.**

| Location ID | Location name | Latitude | Longitude | Bermejo catchment | Distance from mountain front (km) | Year | n | Sample type |
|---|---|---|---|---|---|---|---|---|
| AR20SD01 | Caimancito | -23.7109 | -64.5366 | Southern Headwater *Rio San Francisco* | -22 | 2020 | 2 | Transect |
| AR20SD05 | Rio Colorado | -23.2962 | -64.2191 | Northern Headwater *Upper Rio Bermejo* | -16 | 2020 | 4 | Transect |
| AR20SD02 | Embarcacion | -23.2479 | -64.1375 | Northern Headwater *Upper Rio Bermejo* | -10 | 2020 | 4 | Transect |
| AR20SD03 | Pichanal | -23.3559 | -64.1827 | Southern Headwater *Rio San Francisco* | -15 | 2020 | 13 | Transect |
| AR17MR30 | Pichanal | -23.3559 | -64.1827 | Southern Headwater *Rio San Francisco* | -15 | 2017 | 1 | Single point |
| AR17MR17 | Reserva Natural Formosa | -24.3058 | -61.8345 | Downstream *Rio Bermejo* | 249 | 2017 | 1 | Single point |
| AR20SD15 | Puerto Lavalle | -25.6654 | 60.1282 | Downstream *Rio Bermejo* | 481 | 2020 | 12 | Transect |
| AR20SD18 | El Colorado | -26.3444 | -59.3614 | Downstream *Rio Bermejo* | 584 | 2020 | 8 | Transect |
| AR17MR57 | El Colorado | -26.3444 | -59.3614 | Downstream *Rio Bermejo* | 584 | 2017 | 1 | Single point |
| AR17MR05 | General Mansilla | -26.6613 | -58.6314 | Downstream *Rio Bermejo* | 660 | 2017 | 1 | Single point |

### 2.2 Sampling

During sampling campaigns in 2013, 2015, 2017, 2019 and 2020, we collected headwater and lowland floodplain leaf litter, coarse floating particulate organic matter ($POM_{float}$, >1 cm diameter), paleochannel soils, river bank sediments, suspended sediment, and bedload material in the Rio Bermejo catchment (Table 1, Fig. 1a). Sampling of bedload was curtailed by pandemic travel restrictions coming into force during fieldwork in March 2020.

The sampling sites at Rio Colorado and Embarcacion are located within the northern headwaters ($HW_{North}$), and Caimancito and Pichanal are sampling sites in the southern headwaters ($HW_{South}$) along the Rio San Francisco (Fig. 1a). We sampled the Rio Bermejo main stem at five separate locations between the upstream most sampling at Carboncito (14 km linear distance

https://doi.org/10.5194/egusphere-2023-2485
Preprint. Discussion started: 13 November 2023


downstream of the mountain front confluence), and downstream most sampling at General Mansilla (660 km linear distance downstream of the mountain front confluence) (Fig. 1, Table 1).

#### 2.2.1 Bedload sampling: $POM_{Bed}$

In March 2020, we collected bedload material from cross-channel transects (Fig. 2a) at four locations upstream of the Bermejo-San Francisco confluence. At $HW_{South}$, we sampled the Rio San Francisco at Pichanal (n=13) and at Caimancito (n=2). At $HW_{North}$, we sampled the upper Rio Bermejo at Embarcacion (n=10), and the Rio Colorado tributary (n=4) (Fig. 1). Downstream of the confluence, we sampled the lowland Rio Bermejo mainstem at Puerto Lavalle (n=12), 481 linear km downstream of the confluence, and at El Colorado (n=8), 583 linear km downstream of the confluence (Table 1).

We collected bedload samples with a Helley-Smith bedload sampler with a 100 µm mesh and a 8×8 cm square opening (KC Denmark A/S, 2023). We ballasted the sampler with 12 kg weight to enable sinking to the river bed and attached a rope on both ends of the sampler. We deployed this device systematically from bridges in transects across the cross-sections of the Rio Bermejo and Rio San Francisco (Fig. 2a). We lowered the sampler to touch gently on the riverbed for 60 seconds and then retracted the sampler by manually pulling up the sampler as quickly as possible, usually in less than 15 seconds, to minimize capture of material from shallower water column depths. We additionally collected bedload samples at one location per sampling site for a longer period, usually around 5 minutes, to ensure sampling of a sufficient amount of organic bedload material for compositional analysis. The wet samples were stored in air-tight Whirl-Pak plastic bags and transferred to Potsdam, Germany within two weeks. The samples were freeze dried and dry-sieved over a stainless-steel sieve with 1 mm mesh size. Of the 49 bedload samples collected in 2020, 30 yielded no or less than one gram of macroscopic organic material ($POM_{Bed}$), many from downstream sampling sites. For selected samples with abundant organic debris in both fractions, we processed and analyzed the organic bedload material following the protocol described in Sect. 3.2 for both the >1 mm and <1 mm size fractions separately. We found no significant differences between the two size fractions, and therefore analyzed the remaining bedload samples as bulk.

In earlier sampling campaigns, we collected individual bedload samples throughout the catchment (Table 1): In March 2017, we collected single-point bedload samples with a self-built device at one headwater site, Pichanal (Rio San Francisco), and three mainstem Rio Bermejo sites: Reserva Natural Formosa, El Colorado, General Mansilla (Fig. 1a). Six bedload samples collected in November 2019 were collected with a bedload grab and did not yield enough OM to permit compound-specific stable isotope measurements or significant amounts of $POM_{Bed}$. The sampling in these earlier campaigns were performed under qualitative aspects and are therefore not used for a quantitative $POM_{Bed}$ estimation.

The maximum size of the bedload samples was likely limited by the funnel opening width of 8 cm, as has been demonstrated for clastic bedload (Bunte et al., 2008)and limits our sample collection to the material transported within 8 cm above the bed, though it is likely that the $POM_{Bed}$ material is transported in a thicker layer above the bed (Repasch et al., 2022; Schwab et al., 2022). Our sample sizes may reflect these limitations of bedload sampling rather than a physical phenomenon. However, these potential sampling biases do not affect the composition of the sample material.

https://doi.org/10.5194/egusphere-2023-2485
Preprint. Discussion started: 13 November 2023


### 2.2.2 Leaf litter and $POM_{float}$

During campaigns in 2015, 2019, and 2020, we collected 17 leaf litter samples within the floodplain ranging in elevation from 138 to 271 m asl., and 11 total leaf litter samples from $HW_{North}$ and $HW_{South}$ upstream of the Rio Bermejo – Rio San Francisco confluence, between 317 – 854 m asl (Fig. 1). We typically collected ~20 g of leaf litter, the samples were air dried in the field and stored in paper bags upon arrival at the laboratory in Potsdam, Germany. There, the samples were oven-dried at 40°C for up to three days, and stored until further analysis.

We collected seven samples of floating, coarse particulate organic matter ($POM_{float}$, > 1 mm) along the Rio San Francisco (one at 313 m asl and another at 2458 m asl) during the high flow season in March 2013 (Fig. 1a). $POM_{float}$ was collected with an aquarium net (mesh size 1 mm), held into the river water from the river banks until a sufficient amount of organic material was accumulated, and contained organic and inorganic debris ranging from 1 mm to 10 cm. The sample material was intermittently stored in plastics bags and freeze-dried upon returning to the laboratory. The dry sample masses ranged from 5 to 40 g.

### 2.2.3 Soil, bank and suspended sediment

During our campaigns in 2019 and 2020, we collected 15 sediment and 24 soil samples from the river banks and from a paleochannel on the Rio Bermejo megafan, at elevations of ~60 to 390 m asl. We used a rinsed, stainless-steel shovel to collect material from 0 to 20 cm below surface. The samples were stored in paper bags and air dried in the field. Upon returning to the laboratory, we oven-dried all samples at 45°C for up to three days, and transferred them into brown glass bottles before analysis. We also include data on suspended sediment particulate organic carbon abundance and composition in the Rio Bermejo from previous studies (Repasch et al., 2021; 2022). Briefly, 48 samples were collected from several locations spanning $HW_{South}$, $HW_{North}$, and the lowland Rio Bermejo downstream to General Mansilla, near the confluence with the Rio Paraguay (Fig. 1a).

## 3 Analysis and preliminary data

### 3.1 Near-bed flow velocity and channel depths

During the 2020 campaign, we determined the flow velocity and channel depth at the sampling locations at Embarcacion and Pichanal near the confluence, and downstream at Puerto Lavalle and El Colorado. Surveys were conducted from bridges using an Acoustic Doppler Current Profiler (ADCP; Sontek RiverSurveyor RS-M9) and the raw data was processed using the SonTek RiverSurveyor Live Software (Version 4.1). After quality assessment in the SonTek Software, we further processed the data files using the velocity mapping toolbox (v.4.09) (Parsons et al., 2013) to calculate smoothed mean cross sections with the river flow velocity determined at horizontal and vertical grid node spacing of 1 m and 0.5 m, respectively. We extracted the river depth and flow velocity at each bedload sampling point by overlaying our GPS data points with these cross sections. To

https://doi.org/10.5194/egusphere-2023-2485
Preprint. Discussion started: 13 November 2023


approximate the bedload transport velocity, we multiplied the depth-averaged streamwise flow velocity from the ADCP velocity profiles by 0.7 (Chatanantavet et al., 2013).

The ADCP-estimated near-bed flow velocity ranged between -0.17-1.19 m $s^{-1}$ and was on average 0.5 m $s^{-1}$±0.4 m $s^{-1}$ for the ensemble of sampling sites (n=4). We attribute occasionally negative flow velocities to local flow structures on large river bedforms (Allen, 1968), and assign them no general significance (Fig. 2b). River depths measured during the wet season varied between 8.1-8.5 m at Pichanal and Embarcacion, 1.9-9.9 m at Puerto Lavalle, and 2.4-8.4 m at El Colorado (Table S1). Due to the interrupted campaign in March 2020, these values do not cover the braided section of the river in the upper part of the east Andean foreland.

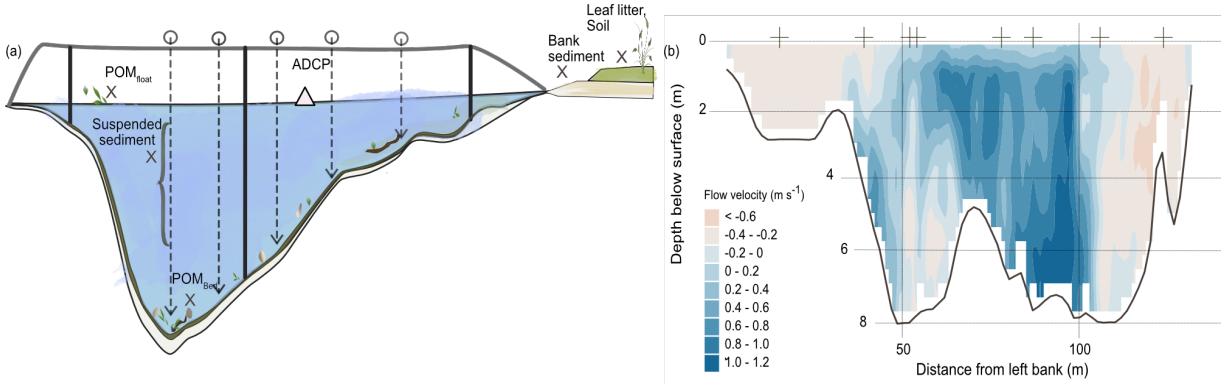


**Figure 2: (a) Schematic channel cross section with transect sampling points (arrows), sample types used in this study, and indicated sample locations. (b) Cross-channel velocity profile using Acoustic Doppler Current Profiler at the El Colorado station, crosses indicating each transect sampling point at the El Colorado station. Bridge pillars were at 30, 75 and 125 m, measurements were taken ~5 m upstream of the bridge.**

The high flow velocities and water depths of the Rio Bermejo made sampling of river bedload difficult, and thus the composition of some samples may have been affected by admixture of suspended load during sampler recovery. This is most likely to occur in the sediment-laden upper reaches of the Rio Bermejo and at downstream sites where bridge pillars cause additional turbulence.

### 3.2 Organic-geochemical analysis and raw results

To fingerprint source areas of the OM collected in this study, we use biomarker proxies, specifically long-chain *n*-alkanes, which are recalcitrant organic molecules that are often preserved in sediments (e.g., Thomas et al., 2021; Cranwell, 1972). Long-chain *n*-alkanes stable carbon and hydrogen isotopes incorporate local environmental conditions at formation, and therefore, can help to track the source areas of POM in river sediment (e.g., Hemingway et al., 2016; Hoffmann et al., 2016; Bouchez et al., 2014; Ponton et al., 2014; Galy et al., 2011; Sachse et al., 2004).

We extracted *n*-alkanes from all samples and measured the compound-specific stable hydrogen and carbon isotope ratios. Soil, bank sediment, suspended sediment and $POM_{Bed}$, samples were ground with a mortar and pestle and lipid compounds were

https://doi.org/10.5194/egusphere-2023-2485
Preprint. Discussion started: 13 November 2023


extracted with 9:1 methanol:dichloromethane, using a ThermoFisher Dionex Accelerated Solvent Extraction system (ASE 350). The non-polar *n*-alkane fraction was separated from the total lipid extract over silica gel columns with glass fiber filters at the base and top (pore size 60 Å, 230–400 mesh particle size) by automated solid-phase extraction (SPE) with a Gilson ASPEC GX-271 and *n*-hexane as solvent, following procedures described by (Rach et al., 2020). *n*-alkanes were extracted manually from leaf litter and $POM_{float}$ by immersing between 0.2 and 10.0 g of the dried samples in a 9:1 methanol:dichloromethane mixture and placing them into an ultrasonic bath at 40°C for 20 to 40 minutes. The *n*-alkanes were separated from the total liquid extract by solid phase extraction (SPE) over a silica gel-equipped 6 mL glass column (Macherey-Nagel, Düren, Germany) using *n*-hexane as solvent (Rach et al., 2020). The solid parts stayed behind and samples were rinsed properly with 9:1 DCM/MeOH. The lipid containing solvents were dried in the TurboVap and the lipids transferred to a smaller vial in approximately 1.5 ml 9:1 DCM/MeOH. The solvents of the TLE were evaporated again with N2 gas and the samples dissolved in 1.5 ml n-hexane. To quantify *n*-alkane concentrations per sample, we added an internal standard, 5α-androstane (10 $\mu$g), and measured the samples in an Agilent gas chromatograph (GC 7890-A) with a flame ionization detector (FID) and a coupled single quadrupole mass spectrometer (MS 5975-C).

We quantified the abundances of *n*-alkane homologues relative to the internal standard using the FID chromatograms. We calculated the average chain length ($ACL_{25\text{-}33}$) of the most abundant *n*-alkanes with chain lengths between 25 and 33 as:

$$ACL_{25-33} = \frac{\Sigma(C_n * n)}{\Sigma C_n} \quad (1),$$

where *n* is the number of carbon atoms of each *n*-alkane, and $C_n$ is the concentration of each *n*-alkane with *n* carbon atoms. The subscripts on $ACL_{25\text{-}33}$ refer to the chain length range analyzed. We determined the carbon preference index ($CPI_{25\text{-}33}$) after (Bray and Evans, 1961) for *n*-alkanes with 25 to 33 carbon atoms, using

$$CPI_{25-33} = \frac{1}{2} * \left(\frac{\Sigma C_{25-33odd}}{\Sigma C_{24-32even}} + \frac{\Sigma C_{25-33odd}}{\Sigma C_{26-34even}}\right) \quad (2),$$

where $\Sigma C_{25\text{-}33odd}$ is the sum of the concentration of odd-chained *n*-alkanes with chain lengths between 25-33, concentration, $\Sigma C_{24\text{-}32even}$ the sum of the concentration of even-chained *n*-alkanes with chain lengths between 24-34, and so forth. To measure compound-specific hydrogen and carbon isotope ratios of the *n*-alkanes (expressed as $\delta^2H$, $\delta^{13}C$ values), we used a Trace GC 1310 (ThermoFisher Scientific) connected to Delta V plus Isotope Ratio Mass Spectrometer (IRMS) (ThermoFisher Scientific) following the procedures described by Rach et al. (2020).

*n*-alkane $\delta^2H$ and $\delta^{13}C$ values were measured in duplicates. For each sample run, we measured the *n*-alkane standard-mix A6 (with n-alkane chain lengths ranging from *n*C16-*n*C30) with known $\delta^2H$ values obtained from A. Schimmelmann (Indiana University), for correction and transfer to the VSMOW scale. The H3+ factor from the $^2H$ measurements was 5.9±0.8 mV. The standard deviation for $\delta^2H$ of the standard measurements was 2.3±0.7‰, and the mean standard deviation for the samples

https://doi.org/10.5194/egusphere-2023-2485
Preprint. Discussion started: 13 November 2023


was 1.1±1.6‰. The mean standard deviation for $^{13}C$ measurements of the standard measurements was 0.11±0.06‰, and the mean standard deviation for the samples was 0.15±0.23‰.

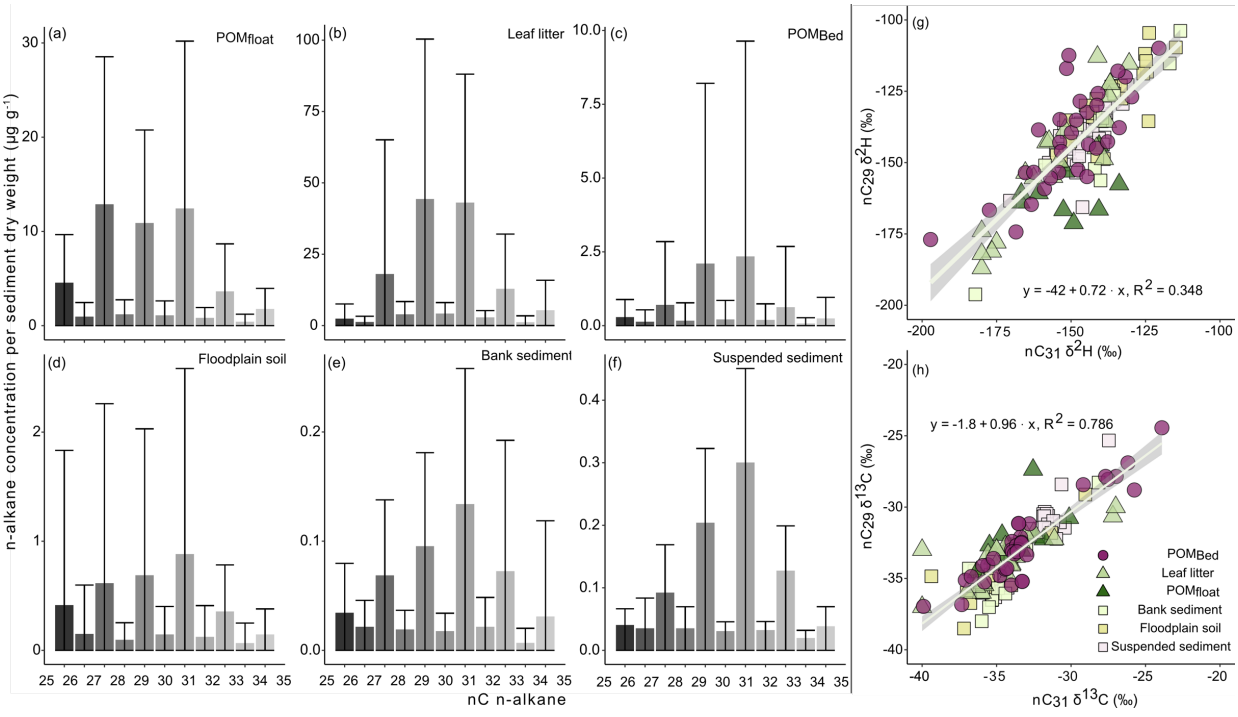


**Figure 3: Left panel (a-f): Average and standard deviation (bars) of the long-chain n-alkane distribution ($nC_{25}$-$nC_{35}$) as concentration per sediment dry weight ($\mu g\ g^{-1}$) of (a) $POM_{float}$, (b) leaf litter, (c) $POM_{Bed}$, (d) floodplain soil, (e) bank sediment and (f) suspended sediment. Note the different y-scale ranges. Right panel (g, h): $nC_{29}$ versus $nC_{31}$ *n*-alkane (g) $\delta^2H$ and (h) $\delta^{13}C$ values of all OM sample types, and linear regression equation and $R^2$ values.**

We calculated the $ACL_{25\text{-}33}$ index for 201 samples collected in the Rio Bermejo catchment, including $POM_{Bed}$, leaf litter, $POM_{float}$, soil, sediment deposits, and river suspended sediment. *n*-alkanes with chain-lengths ranging from $nC_{25}$ – $nC_{35}$ had the highest abundance across all samples (Fig. 3, a-f). The main components were $nC_{31}$, $nC_{29}$ and $nC_{27}$, followed by $nC_{33}$ and $nC_{25}$, while even carbon numbered *n*-alkanes were minor components in all samples. Leaf litter, $POM_{Bed}$ and soil samples had similar concentrations of $nC_{29}$ and $nC_{31}$. In river bank and suspended sediment samples, $nC_{31}$ was the dominant *n*-alkane, whereas $nC_{27}$ was the main component of the $POM_{float}$ samples. We measured the $\delta^2H$ and $\delta^{13}C$ values for the dominant chain lengths, $nC_{29}$ and $nC_{31}$. Because these *n*-alkanes showed a significant correlation for $\delta^{13}C$ ($R^2$ = 0.99) and $\delta^2H$ values ($R^2$ = 0.85, Fig. 3d, h), we will focus on the $nC_{29}$ values.

For a subset of ten $POM_{Bed}$ samples with abundant organic debris in both the >1 mm and <1 mm fractions (Pichanal, Caimancito, Rio Colorado, Embarcacion, and Puerto Lavalle), we analyzed the *n*-alkane composition of $POM_{Bed}$ in both size fractions. In most of these samples, the two size fractions had distinct $ACL_{25\text{-}33}$, $CPI_{25\text{-}33}$, $nC_{29}$ $\delta^2H$ and $nC_{29}$ $\delta^{13}C$ values (Fig. A01). However, no discernible pattern emerged in these differences. For this reason, and because size-specific biomarker

https://doi.org/10.5194/egusphere-2023-2485
Preprint. Discussion started: 13 November 2023


analyses were not possible for smaller sample amounts, we decided to work with *n*-alkane data from the bulk sample material. For samples analyzed as two separate fractions, we determined values for the bulk sample material as the weighted average of the two fractions. These values were dominated by the fraction <1 mm, which had the greater mass in all cases. In the following, we will refer to the results of analyses of the total particulate organic carbon of the sampled bedload material in the full-size range as $POM_{Bed}$.

### 3.3 Data analysis

All data analyses were performed using R 4.1.2 GUI 1.77 High Sierra build (8007). We report the range of the values as average ± standard deviation, and the number of samples. We used the Kolmogorov-Smirnov-Test to account for the non-normal distribution of our data and the Mann-Whitney U test to test for significant differences between independent sample groups. We used linear regression and associated $R^2$ to test for significant trends in our data. The significance level is reported at the 95% confidence interval (p-value < 0.05).

## 4. $POM_{Bed}$ presence, source and ability to survive long distance transport

We aim to answer three questions regarding the source, transport, and survival of $POM_{Bed}$ in the Rio Bermejo. First, we want to observe when and where $POM_{Bed}$ is in active fluvial transport and how $POM_{Bed}$ composition varies throughout the catchment. We then investigate the sources of $POM_{Bed}$ by determining the elevation and climate of the OM source using *n*-alkane $\delta^2H$ values to, assessing the biological variability of $POM_{Bed}$ sources using $\delta^{13}C$ values combined with $ACL_{25\text{-}33}$ to, and assessing $POM_{Bed}$ maturity using $CPI_{25\text{-}33}$. Finally, we apply a mixing model using these geochemical data to define distinct $POM_{Bed}$ sources. Collectively, this approach allows us to evaluate the survival and fate of $POM_{Bed}$ during long-range fluvial transport in the Rio Bermejo.

### 4.1 Is there transport of $POM_{Bed}$ in the lowland Rio Bermejo and what is its geochemical composition?

#### 4.1.1 Bedload mass and material composition

The mass of bedload samples comprising organic and clastic particles was up to an order of magnitude greater at the headwater confluence sites than at the downstream sites for the same sampling procedure. Sampling at Pichanal and Embarcacion yielded totals of 560 g $min^{-1}$ (n = 13), and 259 g $min^{-1}$ (n = 10), respectively, while at Puerto Lavalle we collected a total of 51 g $min^{-1}$ (n = 12), and 77.1 g $min^{-1}$ (n = 8) at El Colorado, respectively (Fig. 4d, Table S1). The mass of dry $POM_{Bed}$ in individual bedload samples varied from 0g to ~20g, without clear spatial patterns. The mass of organic bedload scaled loosely with the amount of clastic sediment collected (Fig. 4d). The material collected in $POM_{Bed}$ samples ranged from fragile, intact leaves and twigs to robust wood fragments with frayed edges and organo-clastic aggregates in the size range from <1 mm to ~10 cm, often mixed with fine organic debris <1 mm (Fig. 4). The organo-clastic aggregates were easily dissociated during sieving, separating into fine sand and silt, and apparently degraded OM particles ranging from <1 mm to >1 cm (Fig. 4).

https://doi.org/10.5194/egusphere-2023-2485
Preprint. Discussion started: 13 November 2023


Chemical maturity of an OM sample can be expressed with the $CPI_{25\text{-}33}$, where lower values indicate a higher sample maturity due to chemical alterations of the OM. The strong predominance of odd-over-even *n*-alkane chain lengths in $POM_{Bed}$ ($CPI_{25\text{-}33}$ average: 7.4±3.0, n = 39, Fig. 5), and the $ACL_{25\text{-}33}$ averaging 29.6±0.9 (range: 27.4-31.6, n =39, Fig. 5) throughout the catchment indicate relatively fresh or little-degraded vascular plant material in the Rio Bermejo bedload (Eglinton and Hamilton, 1967; Bray and Evans, 1961). The occurrence of low $CPI_{25\text{-}33}$ <1 values in our dataset may be due to the occasional presence of burnt OM, such as charcoal particles, in the river bedload. While it is difficult to evaluate the volumetric contribution of this low $CPI_{25\text{-}33}$ material, it is negligible relative to other $POM_{Bed}$ sources.

The $POM_{Bed}$ fraction <1 mm consisted of mixed organic debris and clastic sediment and the coarser fraction >1 mm was composed predominantly of organic debris. Only the location at Pichanal at the Rio San Francisco carried substantial amounts of pebbles in the fraction >1 mm, and organo-clastic aggregates were more abundant at downstream sites. The geochemical analysis also revealed substantial differences in the size fractions >1 and <1 mm $POM_{Bed}$ in nearly all samples with sufficient


**Figure 4: Examples of captured $POM_{Bed}$ as (a) bulk fraction from the Rio San Francisco at Pichanal, (b) Rio Bermejo at Puerto Lavalle, in particle size separates: >1 mm, aggregated (left) and dissociated (middle), and <1 mm mixed with clastic material, (c) bulk at the Rio Bermejo at Embarcacion, and (d) sampled bulk bed material (empty symbols) and $POM_{Bed}$ > 1 mm (filled symbols) per sampling point at all sampling locations. Note the unequal x-axis breaks, and that $POM_{Bed}$ > 1 mm is shown in in g min$^{-1}$, and bulk bed material in in g min$^{-1}$ x10$^{-1}$, to account for the mass difference of the samples.**

mass for an articulated analysis (Figure S1). The compositional differences between size fractions, as measured in our limited sample set, lack any discernible systematics, suggesting that variable sourcing affects both size fractions. Variable proportions of woody debris versus leaf fragments, biogeochemical quality, and size distribution indicate significant variability in the sourcing of materials of different sizes at each sampling location of $POM_{Bed}$ even within a single site (Fig. A01b, f). This implies that OM fragments in the Rio Bermejo bedload have diverse histories and indicates incomplete mixing both across the channel and along the length of the river, possibly due to highly active floodplain migration in some parts of the channel.

Geochemically, the similarity of $POM_{float}$, leaf litter, soils, sediments, and $POM_{Bed}$ suggests it is the source of the sampled $POM_{Bed}$ and no major transformations have occurred during fluvial transit (Fig. 5). Leaf litter and soil inputs from hillslope

https://doi.org/10.5194/egusphere-2023-2485
Preprint. Discussion started: 13 November 2023


and riparian areas have potential to be important sources adding to the $POM_{Bed}$ from the headwaters, yet, the sampled soils contained little to no coarse POM, suggesting that eroded soil is more likely to become river suspended sediment than $POM_{Bed}$. Therefore, $POM_{float}$ and leaf litter are likely more important contributors to the $POM_{Bed}$ load. Another presumable $POM_{Bed}$ source is abundant woody debris in the catchment; however, this material contains insufficient *n*-alkanes to perform the same analysis. $POM_{Bed}$ $CPI_{25\text{-}33}$ values (average: 7.4±3.0, n = 39) were not significantly different from leaf litter (7.4 ±4.0, range:1.0-19.8, n = 28), soils (5.9±3.6, range: 0.2-16.3, n = 29) and river bank sediments (6.5±3.7, range: 0.3-13.7, n = 18). However, on average $POM_{Bed}$ $CPI_{25\text{-}33}$ values were lower than soils, bank and suspended sediment (5.5±1.0, range: 1.1-7.8; n = 41), indicating a lower maturity of $POM_{Bed}$. $CPI_{25\text{-}33}$ values of $POM_{float}$ were substantially higher than all sediment samples (15.0±8, range: 2.4-27.9, n = 6), indicating it was, on average, less degraded than other sampled OM.

Before we go analyze the details of $POM_{Bed}$ sourcing, we discuss the mechanisms of $POM_{Bed}$ recruitment.

#### 4.1.2 Mechanisms of recruitment and transport of $POM_{Bed}$

$POM_{Bed}$ is ubiquitous in the bedload of the Rio Bermejo throughout the catchment during the high flow season (Dec-Apr), when the South American Monsoon drives intense precipitation events throughout the study area. In contrast, we did not recover significant amounts of $POM_{Bed}$ during the low flow season. The high variability in $\delta^2H$ values from $POM_{Bed}$ sampled in 2017 and 2020, and the lack of significant amounts of $POM_{Bed}$ during the dry season of 2019 suggest that the processes of recruitment and transport occur quickly, possibly on (sub)seasonal timescales. The significantly higher $CPI_{25\text{-}33}$ values of $POM_{float}$ (Fig. 5b) suggest that the degradation of organic debris occurs after it becomes waterlogged. However, aerobic decomposition seems unlikely during active bedload transport, due to the high turbidity and depth of the river water. Instead, fresh plant debris is likely stored intermittently on hillslopes, floodplains or in-stream during the low flow season (May-Nov), where it can be degraded to various extents and waterlogged. With onset of the strong precipitation and high-water levels, it is mobilized by overland flow, hillslope mass wasting, or lateral channel erosion, (e.g., Wohl et al., 2019; Turowski et al., 2016; Smith et al., 2013b; Hilton et al., 2012; Hilton et al., 2008; Selva et al., 2007), and subsequently transported as $POM_{Bed}$ (Turowski et al., 2016) during the high flow season.

https://doi.org/10.5194/egusphere-2023-2485
Preprint. Discussion started: 13 November 2023


In the headwaters, the erosive potential during the high flow season may exceed the production of organic debris in the riparian corridor on a seasonal timescale, limiting the supply of organic debris to the channel (Hilton et al., 2012; Yager et al., 2012; Garcia et al., 1999), and, consequently, the recruitment of $POM_{Bed}$. In this case, $POM_{Bed}$ export may peak early in the high flow season and diminish over the course of the season as the supply of organic debris is progressively reduced with each subsequent rain storm and $POM_{Bed}$ travels steadily downstream, similar to findings of seasonal sourcing of suspended OC at the Rio Bermejo (Golombek et al., 2021).

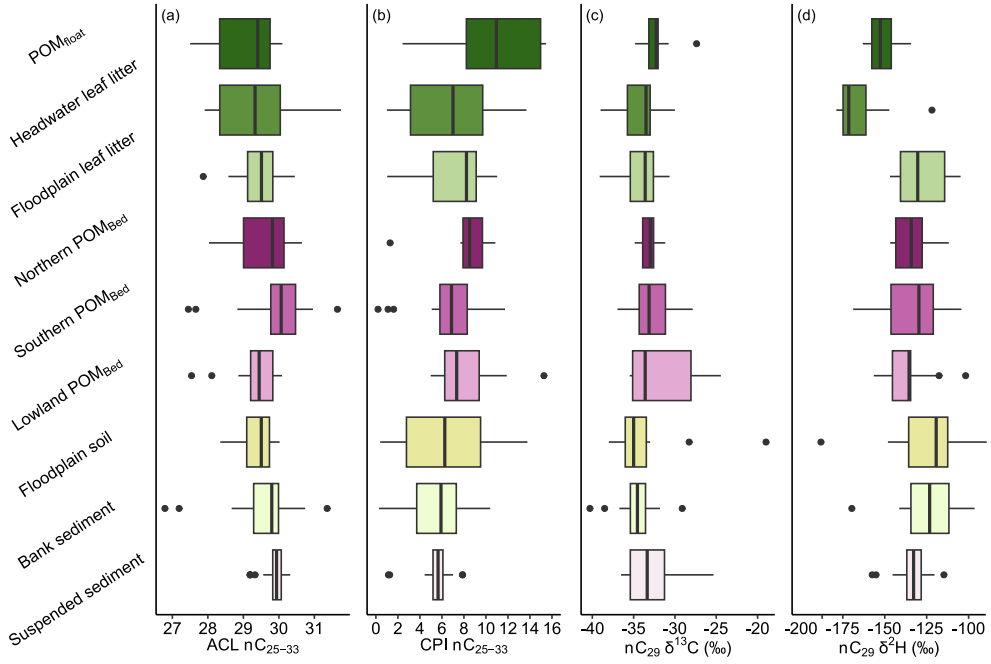


**Figure 5: Summary of (a) $ACL_{25\text{-}33}$, (b) $CPI_{25\text{-}33}$, (c) $nC_{29}$ $\delta^2H$ and (d) $nC_{29}$ $\delta^{13}C$ values of $POM_{float}$, headwater and floodplain leaf litter; $POM_{Bed}$ from the northern headwater, southern headwater and downstream floodplain; floodplain soil, bank sediment, and suspended sediment. Boxplot width shows the interquartile range, black line the median, whiskers minimum and maximum range of the data without outliers. Black dots indicate outliers with 0.75 Quantile + 1.5 x interquartile range and 0.25 Quantile - 1.5 x interquartile range, respectively.**

In the lowland floodplain, $POM_{Bed}$ recruitment is also highly seasonal, but the mechanism of recruitment differs from the steep headwater portion of the catchment (Wohl et al., 2019). Lateral channel migration eats into the floodplain forests, mobilizing large volumes of sediment, soil, leaf litter, and standing biomass with each bank failure. Bank erosion is most active at the peak of high flow season, providing a source of fresh OM to $POM_{Bed}$, and contributing to the poorly mixed nature of $POM_{Bed}$. However, poorly mixed samples could be expected at high rates of lateral migration from the upstream confluence to ca. 400 km downstream, but enhanced mixing seems more likely in segments with less active migration in the furthest downstream reach of the Rio Bermejo. Our results do not indicate enhanced mixing downstream, possibly because of the quick transport timescales, compared to the production and recruitment of $POM_{Bed}$.

https://doi.org/10.5194/egusphere-2023-2485
Preprint. Discussion started: 13 November 2023


Both upland and lowland lateral erosion processes are markedly reduced during the low flow season, aligning with our observations of ubiquitous $POM_{Bed}$ transport in Dec-Apr and negligible $POM_{Bed}$ transport in May-Nov.

### 4.2 What are the source areas for recruitment of $POM_{Bed}$ and does it survive long-range transport?

In the previous section, we concluded that $POM_{Bed}$ is a heterogenous mixture of OM from various sources in the catchment. Here we aim to more quantitatively determine the sources areas that contribute to create $POM_{Bed}$ by building a mixing model with geochemically distinct sources. By understanding the source area and how far traveled $POM_{Bed}$ is, we can determine the transformation and fate of $POM_{Bed}$ during long-range transit.

#### 4.2.1 Mixing model analysis

We defined three potential $POM_{Bed}$ sources, from coarse organic debris we sampled at distinct elevations in the catchment: floodplain leaf litter (<320 m), headwater leaf litter (320-1000 m) and headwater $POM_{float}$ (>320 m). We use the average and standard deviation of the $ACL_{25\text{-}33}$, $nC_{29}$ $\delta^{13}C$ and $nC_{29}$ $\delta^{2}H$ values (Fig. 6a, b) to constrain source mixing regions after (Smith et al., 2013a). In short, the model uses Monte Carlo simulations to iterate convex hulls that demonstrate the probability that our observed $POM_{Bed}$ samples can be explained by the proposed mixing model, using the point-in-polygon assumption. We assumed uniform source mixing of the $POM_{Bed}$ samples, and no fractionation from the source composition of $POM_{float}$, floodplain, and headwater leaf litter $\delta^{2}H$ /$ACL_{25\text{-}33}$ and $\delta^{2}H$ /$\delta^{13}C$ to $POM_{Bed}$. We used minimum and maximum boundary conditions based on our source data: 25 to 35 for the $ACL_{25\text{-}33}$, -110 and -180‰ for $\delta^{2}H$, and -10 and -40‰ for $\delta^{13}C$ values. We used a resolution of 500 for the mixing region, with 3000 iterations. The resulting mixing regions were not sensitive to variations of the boundary conditions. The variance of the convex hull area stabilized after ~1000 iterations for the $\delta^{2}H$ /$ACL_{25\text{-}33}$ model, at a variance of 40 ‰$^2$, and after ~1000 iterations for $\delta^{2}H$ /$\delta^{13}C$ at a variance of 60 ‰$^2$. The results are plotted as derived mixing regions, with different levels of confidence representing the likelihood of which the observed data can result from mixing of the source data (Fig. 6).

#### 4.2.2 Biomarker stable isotope insights into $POM_{Bed}$ source areas

The stable carbon and hydrogen isotope composition of long-chain *n*-alkanes are used in paleoclimate research to reconstruct continental paleo vegetation (e.g., Sachse et al., 2012b; Huang et al., 2007; Schefuss et al., 2005; Freeman and Colarusso, 2001), or to deduce environmental conditions and potential sources of OM (e.g., Hemingway et al., 2016; Bouchez et al., 2014; Galy et al., 2011; Sachse et al., 2004). Building off these approaches, we use $ACL_{25\text{-}33}$, $nC_{29}$ $\delta^{13}C$ and $\delta^{2}H$ isotope composition (Fig. 5) of catchment OM to determine the source areas of $POM_{Bed}$ in the Rio Bermejo catchment.

https://doi.org/10.5194/egusphere-2023-2485
Preprint. Discussion started: 13 November 2023


390 *n*-alkane $\delta^{13}C$ values in plants are controlled by the plant metabolism type, with C3 plants around -37 - -27‰ and C4 plants around -22 - -10‰ (e.g., Garcin et al., 2014; Huang et al., 2007; Freeman and Colarusso, 2001; Collister et al., 1994). Rio Bermejo $POM_{Bed}$ $nC_{29}$ $\delta^{13}C$ values ranged averaged -32.4±2.9 (range: -36.9 - -24.4‰, n = 35, Fig. 5d), reflecting an overall

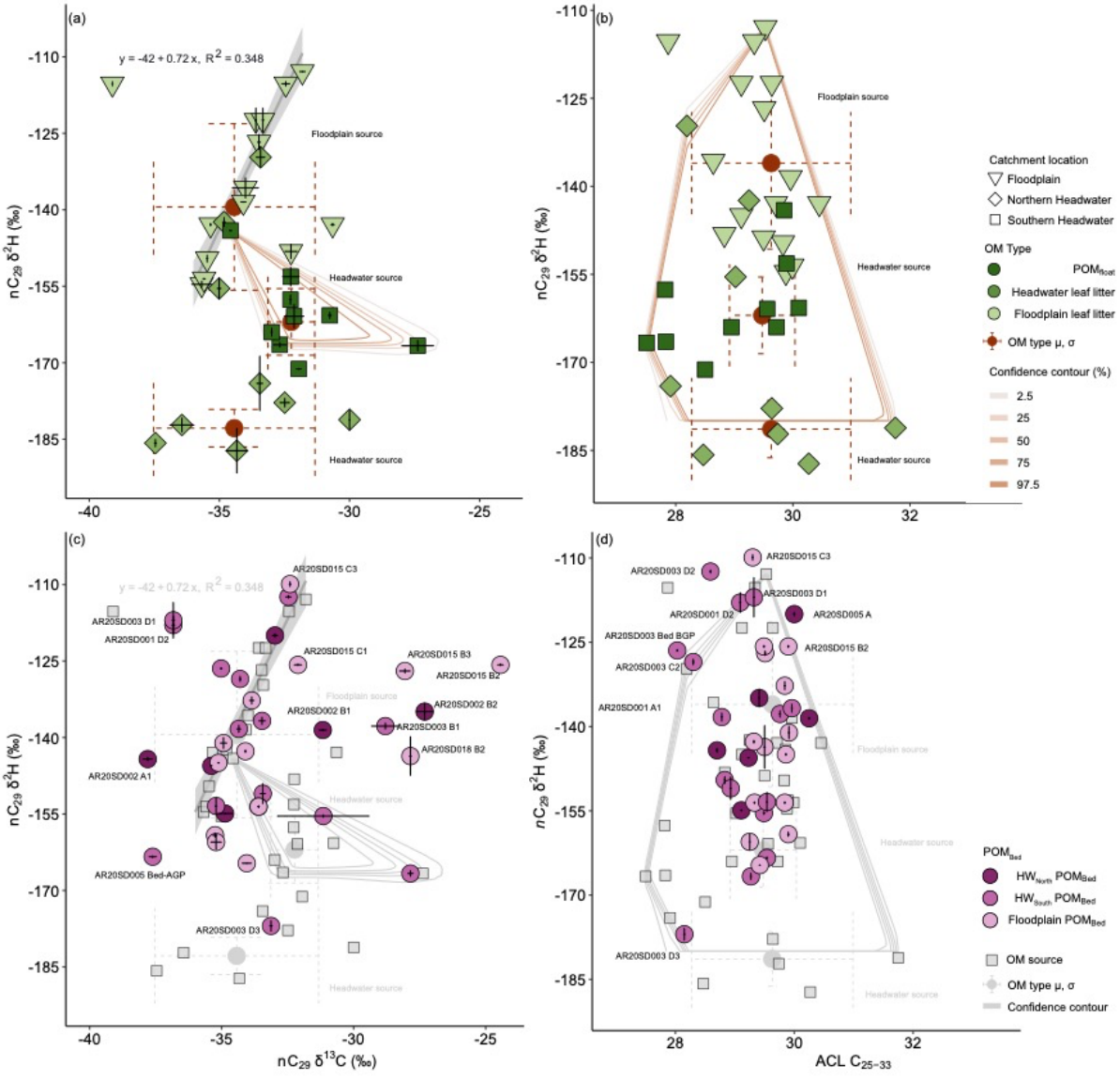


**Figure 6: Upper panel: Headwater and floodplain leaf litter and $POM_{float}$ samples. Red dots are average for each sampling group, and crosses indicate standard deviation. Colored lines are probability contours of the simulated mixing region for the source types (Smith et al., 2013a), at the 2.5% (outermost contour), 25, 50, 75 and 97.5% (innermost contour) level. (a) $nC_{29}$ $\delta^2H$ versus $nC_{29}$ $\delta^{13}C$, and (b) $nC_{29}$ $\delta^2H$ versus $ACL_{25\text{-}33}$. Lower panel: Greyed out area as describe above, colored symbols are $POM_{Bed}$ samples from headwaters and floodplain, for (a) $nC_{29}$ $\delta^2H$ versus $nC_{29}$ $\delta^{13}C$, and (b) $nC_{29}$ $\delta^2H$ versus $ACL_{25\text{-}33}$. Labelled $POM_{Bed}$ samples are those that fall outside the mixing area and the source area of both plots. Uncertainty is plotted inside the symbol.**

https://doi.org/10.5194/egusphere-2023-2485
Preprint. Discussion started: 13 November 2023


C3-dominated plant input (Garcin et al., 2014). Silva et al. (2011) identified a shift towards C3 vegetation in our study area in the last ~3000 years. This imposes an age cap for the organic bedload material, below which our observation of predominance of fresh to degraded organic material can be accommodated.

There were no distinct differences between the $POM_{Bed}$ $\delta^{13}C$ values and those for catchment soil (-34.5±2.2‰, range: -40.2 - -29.1‰, n = 22), deposited sediment (-33.7±4.5‰, range: -38.0- -18.9‰, n = 16), and floodplain leaf litter (-33.9±2.2‰, range: -39.1 - -30.6‰, n = 15), signaling that all these reservoirs are dominated by C3 inputs (Fig. 5a, c). However, local findings of more positive $\delta^{13}C$ values, and higher $ACL_{25\text{-}33}$ (Fig. 6) suggest C4 plant contributions to $POM_{Bed}$, possibly from maize cultivation in the $HW_{South}$ catchment area (Powell et al., 2012), and to a lesser extent in the lowland reach near El Colorado (Fig. 1b). Because lateral channel migration rates are low in these downstream reaches of the Bermejo (Repasch, 2023; Repasch et al., 2020) it is unlikely that local C4 plants will make it into the bedload in any significant quantities. Finding signatures of C4 plants in lowland downstream bedload samples provides evidence for long-range downstream transport of $POM_{Bed}$ from the Bermejo headwaters to nearly 1000 km downstream.

$n-C_{29}$ $\delta^2H$ values can serve as a proxy for the local meteoric water composition taken up by plants, as it is influenced by the water incorporated into plants during photosynthesis (Sachse et al., 2012a; Hou et al., 2008; Chikaraishi et al., 2004), and are strongly related to temperature, humidity, rainfall amount, moisture source, and elevation (e.g.,Walker and Richardson, 1991; Allison et al., 1984; Stewart and Taylor, 1981). In our study area, increasing altitude causes decreasing $\delta^2H$ values in meteoric water captured in plant tissue: More negative $\delta^2H$ values corresponded to higher elevations. Nieto-Moreno et al. (2016) measured soil $n-C_{29}$ $\delta^2H$ values ranging from -150 to -110‰ in samples collected along a valley transect ranging from ~300 to ~4000 m in elevation at a headwater tributary of the Rio Bermejo between 22 and 24°S, and the same pattern was described for stream water $\delta^2H$ values in this region (Rohrmann et al., 2014). Our samples follow these systematic, with $\delta^2H$ values averaging -136±15‰ (range: -155 - -112‰, n = 13), for leaf litter sampled at ~270 – 320 m elevation in the Chaco lowland, and more negative $\delta^2H$ values in both leaf litter (-168±21‰, range: -187 - -130‰, n = 9) and $POM_{float}$ (-160±7‰, range: -171 - -153‰, n = 5) collected upstream of the confluence.

$^2H$ depletion with increasing elevation correlate significantly in floodplain and headwater leaf litter (Fig. 7), just as the $POM_{float}$ samples, however, with a notably worse fit ($y = -229\text{-}2.1x$, $R^2 = 0.268$). The sampling transects for $POM_{float}$ covers a rapid westward precipitation decline, where samples from >1000 m asl. are likely sourced from arid areas, whereas the samples from lower elevations receive orographic precipitation, suggesting that the gradient in precipitation amount may cause the observed $^2H$ depletion and the worse fit in $POM_{float}$ samples.

Nevertheless, the elevation dependent $\delta^2H$ composition is caused by a precipitation-dependent change in $\delta^2H$ values of the areas covered by our study, as shown by Nieto-Moreno et al. (2016) and Rohrmann et al. (2014): The upland areas are depleted in $^2H$ compared to the Rio Bermejo lowland, where convective precipitation is the main source of moisture (Rohrmann et al., 2014). We take advantage of this elevation dependent trend in source POM $\delta^2H$ values to identify source elevations of the

https://doi.org/10.5194/egusphere-2023-2485
Preprint. Discussion started: 13 November 2023


$POM_{Bed}$ samples, where more negative $\delta^2H$ values indicate a higher elevation origin, and less negative $\delta^2H$ values signal a low elevation floodplain origin. $POM_{Bed}$ samples do not show such a correlation of sampling elevation with $\delta^2H$ values, and we suggest this is due to transport between production and sampling of this material.

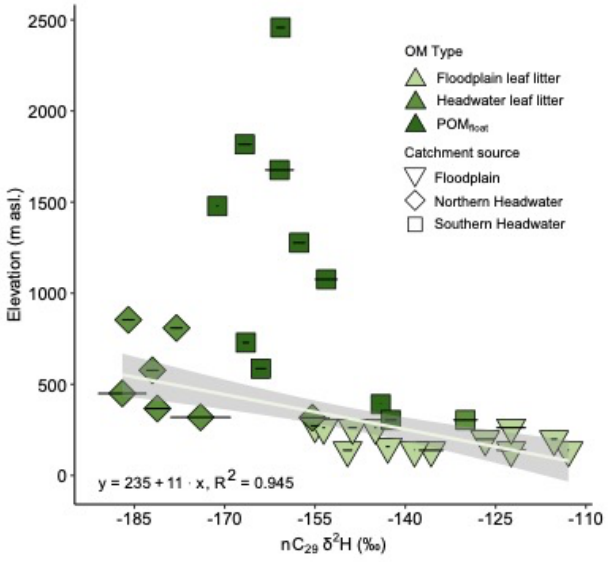


**Figure 7: Sampling elevation and $nC_{29}$ $\delta^2H$ values of floodplain and headwater leaf litter, and $POM_{float}$. Colors represent the organic matter type; symbols represent the catchment source area. The linear regression was done using floodplain and headwater leaf litter data. Linear regression of $POM_{float}$ samples is not shown and shows a significant correlation (p < 0.05; -229-2.1x, R2 = 0.268). $POM_{Bed}$ does not follow this trend. Measurement uncertainty is plotted inside the symbol.**

### 4.2.3 Mixing model insights into $POM_{Bed}$ source areas

We proceed to use floodplain leaf litter, headwater leaf litter, and headwater $POM_{float}$ $ACL_{25\text{-}33}/nC_{29}$ $\delta^2H$, $nC_{29}$ $\delta^{13}C/nC_{29}$ $\delta^2H$ values as potential sources to create mixing regions to fingerprint $POM_{Bed}$ samples (Fig. 6a, b). Most $POM_{Bed}$ samples fall outside the $\delta^2H/\delta^{13}C$ mixing region, and rather follow $\delta^2H/\delta^{13}C$ trend of leaf litter composition ($y = -22x + 0.08$, $R^2 = 0.94$), $nC_{29}$ $\delta^2H$ values ranging from -174 - -112‰, and $\delta^{13}C$ values ranging from -39.0‰ - -30.0‰ (Fig. 6c). This indicates that floodplain leaf litter is an important source to the sampled $POM_{Bed}$, as already suggested earlier, and that this lowland-derived plant material is not mixed within the bedload, but purely resembles floodplain leaf litter. The altitudinal range of the floodplain samples is less than 300 m over the >800 km long mainstem floodplain, making it unlikely that altitudinal affects cause this downstream trend on isotopic composition. A smaller number of the $POM_{Bed}$ samples fall within the headwater source ranges, and the mixing region, respectively. Combined, this suggests input from at least one high elevation upland source. Evidence for this high elevation OM source in lowland $POM_{Bed}$ samples suggests once again that this OM can survive long-range bedload transport in the Rio Bermejo.

https://doi.org/10.5194/egusphere-2023-2485
Preprint. Discussion started: 13 November 2023


Some $POM_{Bed}$ samples collected from both the headwaters and the lowland fall outside of the source mixing regions constrained by $\delta^2H/\delta^{13}C$ and even the wider region constrained by $\delta^2H$ /$ACL_{25\text{-}33}$ (Fig. 6c, d). These samples have $nC_{29}$ $\delta^2H$ values ranging from -125 - -150‰ and $nC_{29}$ $\delta^{13}C$ values ranging from -27 - -33‰ (see labelled $POM_{Bed}$ samples in Fig. 6). This suggests at least one additional, herein unconstrained source, and the comparably heavy $\delta^{13}C$ values could suggest C4 plant contributions. C4 plants grow only sparsely in the catchment (Fig. 1b), and dominantly due to agricultural land use in $HW_{South}$. We suggest that the missing source in our samples is farmland OM, which would indicate that the $POM_{Bed}$ carbon flux can be directly influenced by anthropogenic land consumption.

Sediment load data from gauging stations on the upper Rio Bermejo and Rio San Francisco indicate that $HW_{North}$ contributes six times more suspended sediment load to the lowland Rio Bermejo than $HW_{South}$ (Repasch et al., 2020). There is a north to south rainfall gradient with almost three times more precipitation in $HW_{North}$ (Fig. 1c, Hijmans et al., 2005), indicating higher erosion potential and possibly causing more recruitment of organic bedload from this area (Galy et al., 2015). This suggests that the $HW_{North}$ source area should dominate organic input from the headwaters.
Even though this cannot be constrained with the geochemical proxies adapted in this study, biomarker and end-member analysis suggest that $POM_{Bed}$ material does survive long-range transport from the headwaters to the lowland floodplain at the Rio Bermejo.

### 4.3 Long-range transport of $POM_{Bed}$

Recent studies show that fresh, coarse organic debris can generally be found towards the river bed (Repasch et al., 2022; Schwab et al., 2022; Feng et al., 2016), but the implications of this transport for the OC cycle are underconstrained. Using our previously described mechanistic understanding of the $POM_{Bed}$ source areas and the evolution downstream, we now interrogate the fate of $POM_{Bed}$ during long-range fluvial transport through the Rio Bermejo floodplain.
The proportion of POM transported at the bed versus in suspension is a function of particle size and shape, the recalcitrance of the POM, the river's turbulence, sediment load, the flow close to the bed (Turowski et al., 2016; Nichols et al., 2000), and secondary flow motions (Schwab et al., 2022). Assuming that $POM_{Bed}$ moves as clastic bedload, with a pace of about 0.7 times the depth-averaged flow velocity (Chatanantavet et al., 2013), we find that coarse OM moves along the river bed at estimated near-bed flow velocity of 0.46 m $s^{-1}$ (average of positive flow velocities, Table S1) at both the Bermejo-San Francisco confluence and downstream locations alike. At this velocity, a $POM_{Bed}$ parcel could be transported 1300 km through the Rio Bermejo floodplain in ~30 days. Moreover, slightly higher $CPI_{25\text{-}33}$ values at downstream sites (average: 8.2±3.0, range 4.9-15.2, n = 14, Fig. 5) versus upstream (average: 6.9±3.0, range 0.1-11.7, n = 25, Fig. 5) suggest there is no systematic, progressive degradation of $POM_{Bed}$ during long-range fluvial transport, likely because transport timescales are too short to produce significant chemical degradation. This demonstrates that $POM_{Bed}$ can travel from the Andean headwaters into the Rio Paraguay within one single high flow season in the Rio Bermejo, which explains the absence of $POM_{Bed}$ during the low flow

https://doi.org/10.5194/egusphere-2023-2485
Preprint. Discussion started: 13 November 2023


season. This also explains its occurrence in turbidity currents and turbidite deposits, where coarse POM is buried under finer organo-clastic sediments (Hage et al., 2020; Lee et al., 2019; McArthur et al., 2016; Sparkes et al., 2015).

Once entrained, $POM_{Bed}$ likely moves as semi-separate layer in deep and fast flowing parts of the channel cross section where bed shear stress is greatest. Without substantial mixing, parcels of $POM_{Bed}$ may shuffle downstream due to discrete erosion events at high flow and deposition at low flow. Episodic flushing events of the channel can transport parcels efficiently (Heijnen et al., 2022), and facilitate waterlogging of the organic debris(West et al., 2011). Waterlogged coarse organic debris is, therefore, not prone to spilling onto the river bank or across levees into adjacent flood basins and can progress downstream. Thus, the downstream advection of $POM_{Bed}$ in the Rio Bermejo may be sustained by seasonal high flow driven by monsoonal rainfall and quasi-uninterrupted by intermittent deposition. The helical flow induced by the constant meandering of the lower Rio Bermejo could augment this process (Schwab et al., 2022). As such, significant amounts of OM could be efficiently transported with bedload through large drainage basins, from mountainous uplands to marine basins on sub-seasonal timescales.

#### 4.3.1 Mechanical comminution of $POM_{Bed}$ during long-range transport

Despite evidence for survival during long-range fluvial transport, we might expect that the physical interaction between bedload OM and clastic particles can cause comminution of organic particles (Dosch et al., 2021; Scheingross et al., 2019; Turowski et al., 2016; Hilton et al., 2012; Attal and Lavé, 2009; Nichols et al., 2000), and that comminuted $POM_{Bed}$ transfers into the river suspended load. The observed decrease in $POM_{Bed}$ sample size with increasing distance downstream from the confluence suggests a progressive loss of $POM_{Bed}$ (Fig. 4d), despite the input of OM from lateral erosion of the lowland floodplain. The similarity between *n*-alkane $\delta^{13}C$, $\delta^{2}H$, and $ACL_{25\text{-}33}$ values of the Rio Bermejo suspended sediment and $POM_{Bed}$ (Fig. 5) implies that the two fractions share an origin. River suspended sediment samples yielded similar $CPI_{25\text{-}33}$ values, on average 5.5±1.0 (range: 1.1-7.8; n = 41), but with less variability and values as high as 7.8, suggesting advanced mixing and maturity compared to $POM_{Bed}$ (average: 29.6±0.9, range 27.4-31.6, n =39).

The particle size distributions of $POM_{Bed}$ samples from downstream locations were considerably finer than samples from the confluence, even if the recovered sample sizes did not permit separation of aliquots for grainsize measurements. As flow velocities increase, $POM_{Bed}$ particles may increasingly transfer into suspension, rather than traveling at the river bed (Turowski et al., 2016). This transition is smooth, and $POM_{Bed}$ may move in saltation at the transition between the two transport modes (e.g., Turowski et al., 2016; Nichols et al., 2000). However, flow velocities along the Rio Bermejo mainstem show no significant variability, therefore, transfer from $POM_{Bed}$ to the suspended load is more likely to result from the comminution of coarse particles, rather than changes in river hydrodynamics.

## 5 Synthesis: Is the $POM_{Bed}$ flux important for the terrestrial carbon cycle?: Bedload carbon fluxes at the Rio Bermejo

https://doi.org/10.5194/egusphere-2023-2485
Preprint. Discussion started: 13 November 2023


We close with a provisional examination of the organic carbon flux associated with bedload transport, its relation to suspended transport, and its role in the terrestrial carbon cycle. We extrapolated our local, high flow season point measurements of $POM_{Bed}$ across the respective river transects, ignoring any OM particles <1 mm in near-bed transport, and used a simple upscaling approach to estimate the flux of organic carbon with bedload.

$$POM_{Bed} = \frac{\overline{POM}_{Bed} \times 0.58}{i} \times \frac{\text{Transect width} \times 0.5}{\text{Funnel width}} \times t_{transport} \quad (3).$$

With the average $\overline{POM}_{Bed}$ ($POM_{Bed}$ (mass × time$^{-1}$) >1 mm, over all sampling points i) along each transect, using the respective standard deviation of $\overline{POM}_{Bed}$ to define an upper and lower boundary of the estimated bedload carbon flux. We estimated the carbon content of $POM_{Bed}$ to be 58% organic carbon by weight using the van Bemmelen factor (Allison, 1965). We upscaled the samples sampled along the width of the sampling funnel opening of 0.08 m, and assumed that $POM_{Bed}$ transport is limited to the central 50% of the river channel (transect width × 0.5, length). Since we did not capture significant amounts of $POM_{Bed}$ during the dry season, we assumed that $POM_{Bed}$ transport only occurs during the six months of the high flow season ($t_{transport}$ = $1.5768 \times 10^7$ seconds) to estimate the $POM_{Bed}$ flux in tC yr$^{-1}$.

Both headwater locations show an increase from the upstream (Rio Colorado and Caimancito, respectively) to the downstream (Embarcacion and Pichanal, respectively) locations, demonstrating the possibility of fast recruitment of $POM_{Bed}$ on short distances. To determine changes in mass flux from the mountain front to the downstream reaches, we compare the combined headwater fluxes to those estimated at downstream sampling sites. The fluxes of $POM_{Bed}$ at the upper Rio Bermejo at Embarcación ($HW_{North}$) and Rio San Francisco at Pichanal ($HW_{South}$) define the flux into the low-gradient portion of the river. We estimate the $POM_{Bed}$ fluxes from $HW_{South}$ and $HW_{North}$ at 926-1138 tC yr$^{-1}$ and 112-188 tC yr$^{-1}$, respectively, for a total of 1038-1326 tC yr$^{-1}$ exported from the headwaters to the lowland reach (Fig. 8, Table 2). Downstream at Puerto Lavalle, we calculate a $POM_{Bed}$ flux of 155-351 tC yr$^{-1}$, while at El Colorado we estimate 19-27 tC yr$^{-1}$.

It is difficult to reconcile the minimum 66% loss of C in bedload between the Bermejo-San Francisco confluence and Puerto Lavalle (865 km transport distance) with the subsequent large apparent 10-fold reduction of the bedload C flux from Puerto Lavalle to El Colorado, over a transport distance of only ~220 km. The downstream increase of $POM_{Bed}$ conglomerates that dissociated into $POM_{Bed}$ <1 mm, could cause an underestimation of the $POM_{Bed}$ >1 mm flux at El Colorado. The discrepancy may further be due to sampling bias (Turowski et al., 2013), bedload flux variability due to bedforms, the formation of OM waves at the channel bed, interspersed with relatively barren intervals (Heijnen et al., 2022), strongly sustained by discharge (e.g., Rickenmann, 2018; Turowski et al., 2016; Reid et al., 1998), and channel geometry (Fogel and Lininger, 2023). Bedload sampling, particularly using Helley-Smith samplers, can be prone to high variability, and we suggest our estimates are an order approximation (Bunte et al., 2008) that likely underestimate the maximum $POM_{Bed}$ transport rate. This could also cause the

https://doi.org/10.5194/egusphere-2023-2485
Preprint. Discussion started: 13 November 2023


flux rates of $HW_{South}$ that exceed the fluxes at $HW_{North}$, despite the higher erosive potential at $HW_{North}$. Higher agricultural activities in $HW_{South}$ could also enhance surface erosion, and with that OM input locally. Despite these uncertainties, this is the first estimate of its kind, and shows that river POM fluxes may be underestimated without considering this bedload OM flux.

**Table 2: Bedload sampling location, number of samples (i) of organic bedload > 1mm per location, the number of $POM_{Bed}$ samples > 1 mm per transect, the fraction of organic bed > 1 mm per location (g), total transect width as estimated by ADCP (m), estimated organic bedload per transect (g $s^{-1}$ $i^{-1}$), extrapolating n samples of 0.08 m (funnel width) over half the channel width, and average ± standard deviation $\overline{POM}_{Bed}$ flux per year and wet season, respectively (=1.58x$10^7$ s) and transect, in (tC $yr^{-1}$), assuming 58% carbon in the organic load.**

| Location name | i | Total bedload (g) | $POM_{Bed}$ >1 mm (g) | Full transect width (m) | $\overline{POM}_{Bed}$ flux (g $s^{-1}$) | Carbon $\overline{POM}_{Bed}$ flux ± standard deviation (tC $yr^{-1}$) |
|---|---|---|---|---|---|---|
| Caimancito | 2 | 588 | 22 | 80 | 94 | 856 ± 513 |
| Embarcacion | 4 | 2589 | 5 | 169 | 16 | 150 ± 38 |
| Pichanal | 11 | 7283 | 66 | 183 | 113 | 1032 ± 106 |
| Rio Colorado | 4 | 955 | 3 | 35 | 1 | 11 ± 1 |
| Puerto Lavalle | 7 | 617 | 9 | 215 | 16 | 253 ± 98 |
| El Colorado | 5 | 617 | 1 | 90 | 1 | 23 ± 4 |

The inferred $POM_{Bed}$ grain size reduction during transport, similar to clastic sediment (Attal and Lavé, 2009), thereby, contributes to the overall suspended sediment yield of the river. The total suspended organic carbon flux is ~$1.85\times10^5$ tC $yr^{-1}$ at the Bermejo-San Francisco confluence (Repasch et al., 2021), suggesting that the estimated $POM_{Bed}$ carbon flux near the confluence is less than 1% of the total carbon load. The Rio Bermejo exports ~$2.24\times10^5$ tC $yr^{-1}$ in suspension downstream to the Rio Paraguay, implying that about $0.39\times10^5$ tC $yr^{-1}$ of suspended organic carbon are delivered to the lowland channel by lateral erosion (Repasch et al., 2021). If we take the downstream estimates of bedload C flux at face, and assume this loss transfers to the suspended load, a mass balance suggests that less than 1% of the suspended load gain between the confluence and Puerto Lavalle and El Colorado could be due to grain size reduction of the coarse organic load.

While our bedload carbon flux estimates are tentative, it is clear that this mode of organic carbon transfer is small in comparison with the fluvial export of organic carbon in the suspended load of the Rio Bermejo. Nevertheless, the Rio Bermejo's suspended sediment yield is exceptionally high (Sambrook Smith et al., 2016), ad this eye-catching feature in rivers and sedimentary deposits could contribute substantially to the overall flux in other river systems with lower suspended sediment yield (Turowski et al., 2016), and in highly erosive headwater streams with short transport distances from recruitment to subsequent deposition and burial (Blair and Aller, 2012; Hilton et al., 2011). This coarse particulate OM may also have a higher probability of preservation and rapid burial in depositional basins, as its particle settling velocity is higher than smaller particles and may be

https://doi.org/10.5194/egusphere-2023-2485
Preprint. Discussion started: 13 November 2023


less prone to resuspension and oxidation. Future work should aim to enhance our understanding of the significance of $POM_{Bed}$ export and burial over varying transport length scales.

## 6 Conclusion

In this study, we investigated the occurrence, recruitment mechanisms, source areas, and the survival of $POM_{Bed}$ during long-range transport, to understand the implications for the terrestrial organic carbon cycle. We found the persistent occurrence of $POM_{Bed}$ along a 1300 km section of the Rio Bermejo in northern Argentina, from the headwaters to its confluence with the Rio Paraguay.

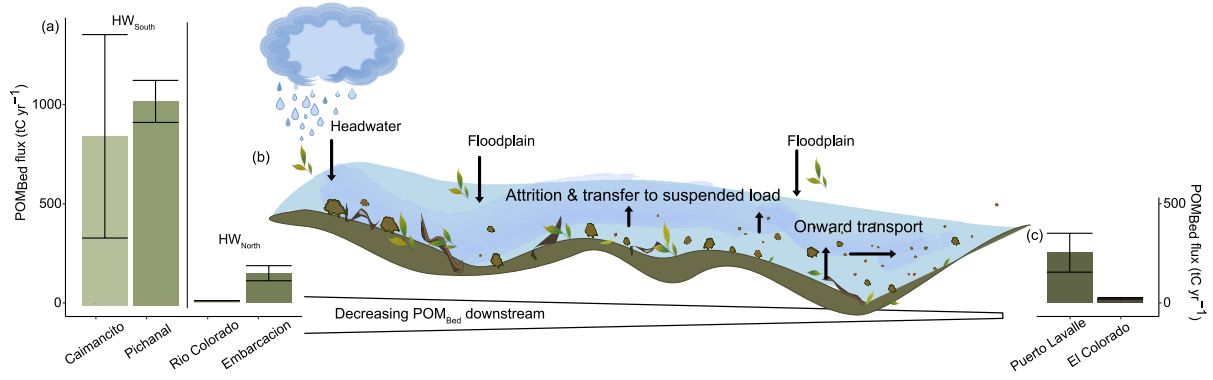


**Figure 8: (a) Bar plot with $POM_{Bed}$ flux (tC $yr^{-1}$ ± standard deviation) at $HW_{South}$ and $HW_{North}$. (b) Illustration of the source areas, transport and fate of $POM_{Bed}$ at the Rio Bermejo from upstream recruitment downstream: Sourcing from the headwater and the floodplain during wet season; erosion, attrition and transfer to suspended load, causing a net decrease in $POM_{Bed}$, and onward transport of the remaining $POM_{Bed}$, leading to (c) $POM_{Bed}$ flux estimates (tC $yr^{-1}$ ± standard deviation) at the downstream at Puerto Lavalle and El Colorado.**

Our results provide evidence that the $POM_{Bed}$ originates from erosion of fresh, terrestrial organic debris from the local floodplain, as well as distal headwater sources, and is a heterogenous mix from catchment-wide sources, dominated by C3 plant input, and local C4 point sources. $POM_{Bed}$ can remain geochemically unaltered over long fluvial transport distances, due to fast transport. The high geochemical variability within and between the bedload sampling transects (Fig. A02) does not allow for a quantitative unmixing of $POM_{Bed}$ sources; however, this suggests that $POM_{Bed}$ may travel in parcels, where each parcel represents an erosive event that delivered fresh OM to the channel, where it was subsequently waterlogged and translocated to the river bed. Our data suggest coherent and continuous transport of individual OM parcels at the river bed, such that $POM_{Bed}$ is never fully mixed longitudinally in a river system. Although $POM_{Bed}$ appears to survive long-range fluvial transport, it can mechanically break down during transport, contributing to the overall suspended sediment load of the river. After physical breakdown, the fate of $POM_{Bed}$ does not lay exclusively in the suspended fraction. The geochemical proxies of the Rio Bermejo soil and bank sediment suggest it can also be stored on floodplains and undergo partial mineralization. Changes in hydraulic settings can lead to particle settling, and high suspended sediment yields enhance the burial efficiency and promote drawdown of atmospheric $CO_2$ over longer timescales.

https://doi.org/10.5194/egusphere-2023-2485
Preprint. Discussion started: 13 November 2023


The decreasing $POM_{Bed}$ flux downstream also indicates that the loss of $POM_{Bed}$ exceeds the recruitment from the floodplain and therefore, that local ecosystem productivity is likely not the main factor controlling $POM_{Bed}$ genesis at the Rio Bermejo. Rather, the main control is likely to be the preconditioning of OM, such that it can rapidly absorb water, increasing its density and its settling velocity, allowing it to sink (Hoover et al., 2010). Overland flow is also necessary to facilitate OM erosion and transport to the active channel, and sufficient river flow velocity is required to maintain transport at the bed (Galy et al., 2015). Likewise, the ratio of $POM_{Bed}$ export and potential burial versus abrasion and transport as suspended sediment likely dependents on plant type, climate, river morphology, hydrodynamics, and transit time (Hoover et al., 2010).

We found that transport of $POM_{Bed}$ is not a major contributor to carbon burial on short timescales at the Rio Bermejo, but ongoing floodplain recruitment contributes to the genesis of $POM_{Bed}$, and fluvial transport could export $POM_{Bed}$ from the headwaters to the ocean on short timescales, representing a hitherto under-investigated mechanism for fluvial organic carbon export and burial. Bedload transport can convey OM to downstream basins with subsequent burial over millennial timescales, however, possibly more significant on shorter transport-distances. The abundance and magnitude of bedload is in general highly variable and notoriously difficult to measure, and it remains challenging to quantify the total amount of $POM_{Bed}$, due to stochasticity of bedload transport and the heterogeneity of $POM_{Bed}$ abundance. Our approach is a first step to evaluate the origin and fate of $POM_{Bed}$ during long-range fluvial transport in a natural setting. Further experimental and field studies are necessary to improve our understanding of the fraction of POM transported as bed material versus in the water column.

https://doi.org/10.5194/egusphere-2023-2485
Preprint. Discussion started: 13 November 2023


## Appendices

610

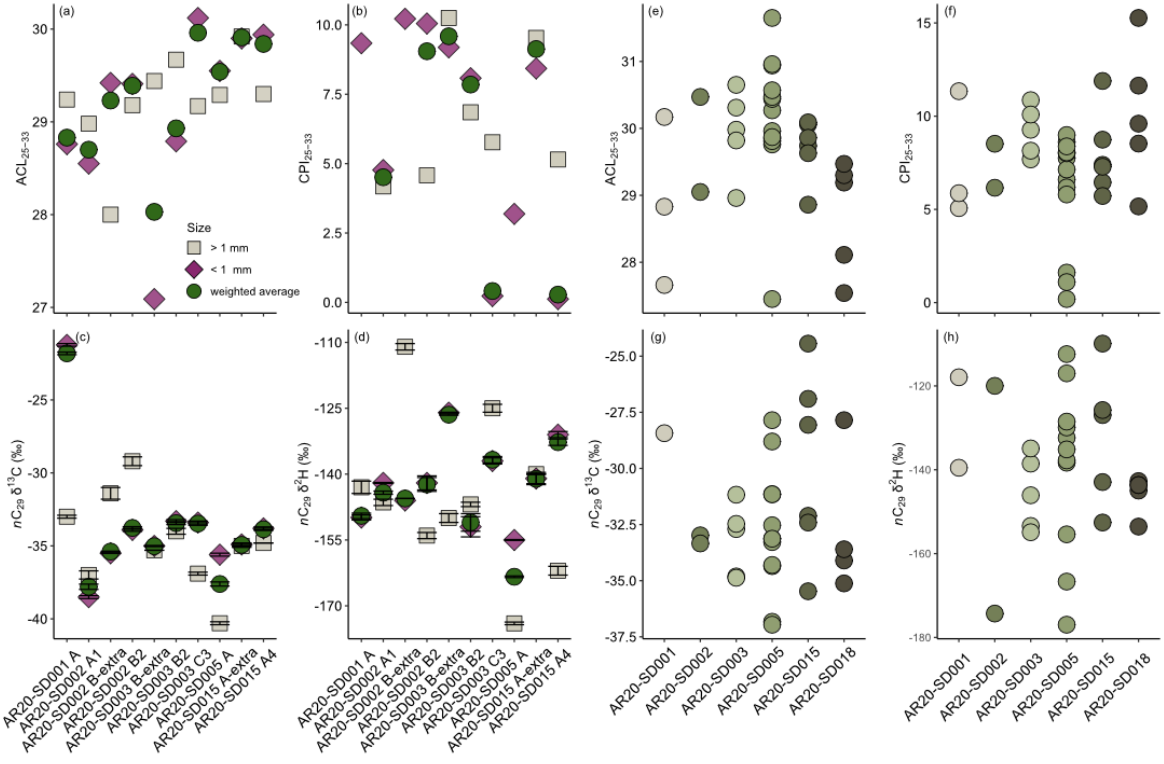


**Figure A01**: **Comparison of subset measurements of $POM_{Bed}$ size fractions larger than 1 mm (> 1 mm), smaller than 1 mm (< 1 mm) and their weighted average of (a) $ACL_{25-33}$, (b) $CPI_{25-33}$, (c) $nC_{29}$ $\delta^{13}C$ and (d) $nC_{29}$ $\delta^{2}H$ values, and bulk (e) $ACL_{25-33}$, (f) $CPI_{25-33}$, (g) $nC_{29}$ $\delta^{13}C$ and (h) $nC_{29}$ $\delta^{2}H$ values of each transect from the wet season campaign, at Rio San Francisco at Caimancito (AR20-SD001) and Pichanal (AR20-SD003), Rio Colorado (AR20-SD005), and Rio Bermejo at Embarcacion (AR20-SD002) and Puerto Lavalle (AR20-SD015) and El Colorado (AR20-SD018).**

https://doi.org/10.5194/egusphere-2023-2485
Preprint. Discussion started: 13 November 2023


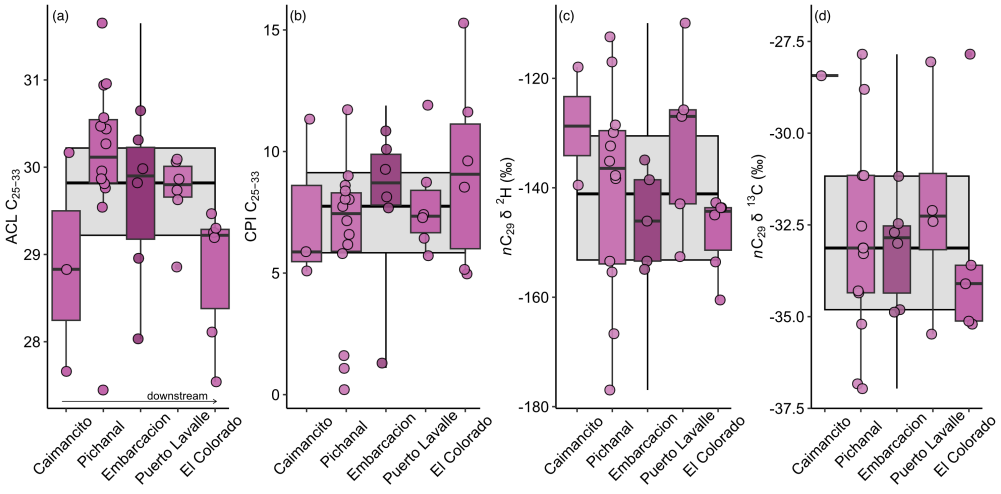


**Figure A02: Boxplots of the $POM_{Bed}$ variability from the (a) $ACL_{25-33}$, (b) $CPI_{25-33}$, (c) nC29 $\delta^2H$, and (d) nC29 $\delta^{13}C$ upstream at Caimancito, Pichanal, Embarcacion, and downstream at Puerto Lavalle and El Colorado. The boxplot in the background includes data from all locations combined. Boxplot width shows the interquartile range, black line the median, whiskers min. and max. range of the data without outliers. Black dots indicate outliers with 0.75 Quantile + 1.5 x interquartile range and 0.25 Quantile - 1.5 x interquartile range, respectively. Colored dots are the individual samples.**

https://doi.org/10.5194/egusphere-2023-2485
Preprint. Discussion started: 13 November 2023


## Data availability

Additional and raw data is can be accesses at https://doi.org/10.5880/GFZ.4.6.2023.005.

## Author Contributions

**Conceptualization:** Sophia Dosch, Niels Hovius, Marisa Repasch, Joel S. Scheingross, Jens Turowski, Dirk Sachse

**Formal analysis:** Sophia Dosch

**Funding acquisition:** Niels Hovius, Dirk Sachse

**Investigation:** Sophia Dosch, Niels Hovius, Marisa Repasch, Stefanie Tofelde, Dirk Sachse

**Methodology:** Marisa Repasch, Niels Hovius, Oliver Rach, Jens Turowski, Dirk Sachse

## Conflicts of Interest

At least one of the (co-)authors is a member of the editorial board of Earth Surface Dynamics.

## Acknowledgments

This research was funded by the Deutsche Forschungsgemeinschaft (DFG) and the Federal State of Brandenburg under the auspices of the International Research Training Group IGK2018 “SuRfAce processes, TEctonics and Georesources: The Andean foreland basin of Argentina” (STRATEGy), DFG grant STR 373/34-1 to M. Strecker. The color scales were taken of Crameri (2021), scientific color maps (doi:10.5281/zenodo.1243862). Figures were produced with R ggplot2, Version 3.4.0.

https://doi.org/10.5194/egusphere-2023-2485
Preprint. Discussion started: 13 November 2023


References

Allen, J. R. L.: Current Ripples. Their relation to patterns of water and sediment motion, Geological Magazine, 106, 614-614, 10.1017/S001675680005946X, 1968.

Allen, G. P., Laurier, D., and Thouvenin, J.: Étude sédimentologique du delta de la Mahakam, Compagnie Française des Pétroles. Notes et Mémoires, 156, 1979.

Aller, R. C.: Mobile deltaic and continental shelf muds as suboxic, fluidized bed reactors, Marine Chemistry, 61, 143-155, https://doi.org/10.1016/S0304-4203(98)00024-3, 1998.

Allison, G. B., Barnes, C. J., Hughes, M. W., and Leaney, F. W. J.: Effect of climate and vegetation on oxygen-18 and deuterium profiles in soils, IAEA, International Atomic Energy Agency (IAEA)1984.

Allison, L. E.: Organic Carbon, in: Methods of Soil Analysis, 1367-1378, https://doi.org/10.2134/agronmonogr9.2.c39, 1965.

Attal, M. and Lavé, J.: Pebble abrasion during fluvial transport: Experimental results and implications for the evolution of the sediment load along rivers, Journal of Geophysical Research, 114, 10.1029/2009jf001328, 2009.

Battin, T. J., Luyssaert, S., Kaplan, L. A., Aufdenkampe, A. K., Richter, A., and Tranvik, L. J.: The boundless carbon cycle, Nature Geoscience, 2, 598-600, 10.1038/ngeo618, 2009.

Berner, R. A.: Burial of organic carbon and pyrite sulfur in the modern ocean- Its geochemical and environmental significance, American Journal of Science, 282, 451-473, 10.2475/ajs.282.4.451, 1982.

Blair, N. E. and Aller, R. C.: The fate of terrestrial organic carbon in the marine environment, Ann Rev Mar Sci, 4, 401-423, 10.1146/annurev-marine-120709-142717, 2012.

Blattmann, T. M., Liu, Z., Zhang, Y., Zhao, Y., Haghipour, N., Montlucon, D. B., Plötze, M., and Eglinton, T. I.: Mineralogical control on the fate of continentally derived organic matter in the ocean, Science, 366, 742-745, 10.1126/science.aax5345, 2019.

Bouchez, J., Galy, V., Hilton, R. G., Gaillardet, J., Moreira-Turcq, P., Pérez, M. A., France-Lanord, C., and Maurice, L.: Source, transport and fluxes of Amazon River particulate organic carbon: Insights from river sediment depth-profiles, Geochimica et Cosmochimica Acta, 133, 280-298, 10.1016/j.gca.2014.02.032, 2014.

Bray, E. E. and Evans, E. D.: Distribution of n-pamlEns as a clue to recognition of source beds, Geochimica et Cosmochimica Acta, 22, 2-15, https://doi.org/10.1016/0016-7037(61)90069-2, 1961.

Bunte, K., Abt, S. R., Potyondy, J. P., and Swingle, K. W.: A Comparison of Coarse Bedload Transport Measured with Bedload Traps and Helley-Smith Samplers, Geodinamica Acta, 21, 53-66, 10.3166/ga.21.53-66, 2008.

Bunte, K., Swingle, K. W., Turowski, J. M., Abt, S. R., and Cenderelli, D. A. A.: Measurements of coarse particulate organic matter transport in steep mountain streams and estimates of decadal CPOM exports, Journal of Hydrology, 539, 162-176, 10.1016/j.jhydrol.2016.05.022, 2016.

Canuel, E. A. and Hardison, A. K.: Sources, Ages, and Alteration of Organic Matter in Estuaries, Annual Review of Marine Science, 8, 409-434, 10.1146/annurev-marine-122414-034058, 2016.

https://doi.org/10.5194/egusphere-2023-2485
Preprint. Discussion started: 13 November 2023


Chatanantavet, P., Whipple, K. X., Adams, M. A., and Lamb, M. P.: Experimental study on coarse grain saltation dynamics in bedrock channels, Journal of Geophysical Research: Earth Surface, 118, 1161-1176, 10.1002/jgrf.20053, 2013.

Chikaraishi, Y., Naraoka, H., and Poulson, S. R.: Hydrogen and carbon isotopic fractionations of lipid biosynthesis among terrestrial (C3, C4 and CAM) and aquatic plants, Phytochemistry, 65, 1369-1381, 10.1016/j.phytochem.2004.03.036, 2004.

Collister, J. W., Rieley, G., Stern, B., Eglinton, G., and Fry, B.: Compound-specific δ 13C analyses of leaf lipids from plants with differing
carbon dioxide metabolisms, Organic Geochemistry, 21, 619-627, https://doi.org/10.1016/0146-6380(94)90008-6, 1994.

Cranwell, P. A.: Chain-length distribution of «-alkanes from lake sedimentsin relation to post-glacial environmental change, Freshwater Biology, 2, 259–265, 1972.

Dellinger, M.: <article-mdd-revised-01-08-23-preprint.pdf>, 2023.

Dosch, S., Hovius, N., Repasch, M., Scheingross, J., Turowski, J., and Sachse, D.: Terrestrial biospheric carbon export from rivers by bedload transport, EGU General Assembly 2021, online, 19–30 Apr 2021, https://doi.org/10.5194/egusphere-egu21-10684,

Feng, X., Feakins, S. J., Liu, Z., Ponton, C., Wang, R. Z., Karkabi, E., Galy, V., Berelson, W. M., Nottingham, A. T., Meir, P., and West, A. J.: Source to sink: Evolution of lignin composition in the Madre de Dios River system with connection to the Amazon basin and offshore, Journal of Geophysical Research: Biogeosciences, 121, 1316-1338, 10.1002/2016jg003323, 2016.

Fogel, C. B. and Lininger, K. B.: Geomorphic complexity influences coarse particulate organic matter transport and storage in headwater streams, Frontiers in Water, 5, 10.3389/frwa.2023.1227167, 2023.

France-Lanord, C. and Derry, L. A.: Organic carbon burial forcing of the carbon cycle from Himalayan erosion, Nature, 390, 65-67, 10.1038/36324, 1997.

Freeman, K. H. and Colarusso, L. A.: Molecular and isotopic records of C4 grassland expansion in the late Miocene, Geochimica et Cosmochimica Acta, 65, 1439–1454, 10.1016/s0016-7037(00)00573-1, 2001.

Galy, V., France-Lanord, C., and Lartiges, B.: Loading and fate of particulate organic carbon from the Himalaya to the Ganga–Brahmaputra delta, Geochimica et Cosmochimica Acta, 72, 1767-1787, 10.1016/j.gca.2008.01.027, 2008.

Galy, V., Peucker-Ehrenbrink, B., and Eglinton, T.: Global carbon export from the terrestrial biosphere controlled by erosion, Nature, 521, 204-207, 10.1038/nature14400, 2015.

Galy, V., Eglinton, T., France-Lanord, C., and Sylva, S.: The provenance of vegetation and environmental signatures encoded in vascular plant biomarkers carried by the Ganges–Brahmaputra rivers, Earth and Planetary Science Letters, 304, 1-12, 10.1016/j.epsl.2011.02.003, 2011.

Garcia, C., Laronne;, J. B., and Sala, M.: Variable source areas of bedload in a gravel-bed stream, J Sediment Res, 69, 27-31, 1999.

Garcin, Y., Schefuß, E., Schwab, V. F., Garreta, V., Gleixner, G., Vincens, A., Todou, G., Séné, O., Onana, J.-M., Achoundong, G., and Sachse, D.: Reconstructing C 3 and C 4 vegetation cover using n -alkane carbon isotope ratios in recent lake sediments from Cameroon, Western Central Africa, Geochimica et Cosmochimica Acta, 142, 482-500, 10.1016/j.gca.2014.07.004, 2014.

https://doi.org/10.5194/egusphere-2023-2485
Preprint. Discussion started: 13 November 2023


Golombek, N., Scheingross, J. S., Repasch, M. N., Hovius, N., Sachse, D., Lupker, M., Eglinton, T. I., Menges, J., Haghipour, N., Poulson, S. R., Gröcke, D. R., Latosinski, F. G., and Szupiany, R. N.: Seasonal variability of fluvial organic carbon composition between 2016-2018 in the Río Bermejo, Argentina, 10.1594/PANGAEA.932558, 2021.

Hage, S., Galy, V. V., Cartigny, M. J. B., Acikalin, S., Clare, M. A., Gröcke, D. R., Hilton, R. G., Hunt, J. E., Lintern, D. G., McGhee, C. A., Parsons, D. R., Stacey, C. D., Sumner, E. J., and Talling, P. J.: Efficient preservation of young terrestrial organic carbon in sandy turbidity-current deposits, Geology, 48, 882-887, 10.1130/g47320.1, 2020.

Hage, S., Galy, V. V., Cartigny, M. J. B., Heerema, C., Heijnen, M. S., Acikalin, S., Clare, M. A., Giesbrecht, I., Gröcke, D. R., Hendry, A., Hilton, R. G., Hubbard, S. M., Hunt, J. E., Lintern, D. G., McGhee, C., Parsons, D. R., Pope, E. L., Stacey, C. D., Sumner, E. J., Tank, S., and Talling, P. J.: Turbidity currents can dictate organic carbon fluxes across river-fed fjords: An example from Bute Inlet (BC, Canada), Journal of Geophysical Research: Biogeosciences, 10.1029/2022jg006824, 2022.

Hayes, J. M., Strauss, H., and Kaufman, A. J.: The abundance of 13C in marine organic matter and isotopic fractionation in the global biogeochemical cycle of carbon during the past 800 Ma, 1999.

Heijnen, M. S., Clare, M. A., Cartigny, M. J. B., Talling, P. J., Hage, S., Pope, E. L., Bailey, L., Sumner, E., Lintern, D. G., Stacey, C., Parsons, D. R., Simmons, S. M., Chen, Y., Hubbard, S. M., Eggenhuisen, J. T., Kane, I., and Hughes Clarke, J. E.: Fill, flush or shuffle: How is sediment carried through submarine channels to build lobes?, Earth and Planetary Science Letters, 584, 10.1016/j.epsl.2022.117481, 2022.

Hemingway, J. D., Schefuß, E., Dinga, B. J., Pryer, H., and Galy, V. V.: Multiple plant-wax compounds record differential sources and ecosystem structure in large river catchments, Geochimica et Cosmochimica Acta, 184, 20-40, 10.1016/j.gca.2016.04.003, 2016.

Hijmans, R. J., Cameron, S. E., Parra, J. L., Jones, P. G., and Jarvis, A.: Very high resolution interpolated climate surfaces for global land areas, International Journal of Climatology, 25, 1965-1978, 10.1002/joc.1276, 2005.

Hilton, R. G. and West, A. J.: Mountains, erosion and the carbon cycle, Nature Reviews Earth & Environment, 1, 284-299, 10.1038/s43017-020-0058-6, 2020.

Hilton, R. G., Galy, A., and Hovius, N.: Riverine particulate organic carbon from an active mountain belt: Importance of landslides, Global Biogeochemical Cycles, 22, n/a-n/a, 10.1029/2006gb002905, 2008.

Hilton, R. G., Galy, A., Hovius, N., Horng, M.-J., and Chen, H.: Efficient transport of fossil organic carbon to the ocean by steep mountain rivers: An orogenic carbon sequestration mechanism, Geology, 39, 71-74, 10.1130/g31352.1, 2011.

Hilton, R. G., Galy, A., Hovius, N., Kao, S.-J., Horng, M.-J., and Chen, H.: Climatic and geomorphic controls on the erosion of terrestrial biomass from subtropical mountain forest, Global Biogeochemical Cycles, 26, 10.1029/2012gb004314, 2012.

Hoffmann, B., Feakins, S. J., Bookhagen, B., Olen, S. M., Adhikari, D. P., Mainali, J., and Sachse, D.: Climatic and geomorphic drivers of plant organic matter transport in the Arun River, E Nepal, Earth and Planetary Science Letters, 452, 104-114, 10.1016/j.epsl.2016.07.008, 2016.

Hoover, T. M., Marczak, L. B., Richardson, J. S., and Yonemitsu, N.: Transport and settlement of organic matter in small streams, Freshwater Biology, 55, 436-449, 10.1111/j.1365-2427.2009.02292.x, 2010.

https://doi.org/10.5194/egusphere-2023-2485
Preprint. Discussion started: 13 November 2023


Hou, J., D'Andrea, W. J., and Huang, Y.: Can sedimentary leaf waxes record D/H ratios of continental precipitation? Field, model, and experimental assessments, Geochimica et Cosmochimica Acta, 72, 3503-3517, 10.1016/j.gca.2008.04.030, 2008.

Huang, Y., Clemens, S. C., Liu, W., Wang, Y., and Prell, W. L.: Large-scale hydrological change drove the late Miocene C4 plant expansion in the Himalayan foreland and Arabian Peninsula, Geology, 35, 10.1130/g23666a.1, 2007.

Iroumé, A., Ruiz-Villanueva, V., and Salas-Coliboro, S.: Fluvial transport of coarse particulate organic matter in a coastal mountain stream of a rainy-temperate evergreen broadleaf forest in southern Chile, Earth Surface Processes and Landforms, 45, 3216-3230, 10.1002/esp.4961, 2020.

Kao, S. J., Hilton, R. G., Selvaraj, K., Dai, M., Zehetner, F., Huang, J. C., Hsu, S. C., Sparkes, R., Liu, J. T.,

KC Denmark A/S: Helley-Smith Sampler: https://www.kc-denmark.dk/products/sediment-trap-station/helley-smith-sampler.aspx, last access: 20.09.2023.

Lee, T. Y., Yang, J. Y. T., Galy, A., Xu, X., and Hovius, N.: Preservation of terrestrial organic carbon in marine sediments offshore Taiwan: mountain building and atmospheric carbon dioxide sequestration, Earth Surface Dynamics, 2, 127-139, 10.5194/esurf-2-127-2014, 2014.

Lee, H., Galy, V., Feng, X., Ponton, C., Galy, A., France-Lanord, C., and Feakins, S. J.: Sustained wood burial in the Bengal Fan over the last 19 My, Proc Natl Acad Sci U S A, 116, 22518-22525, 10.1073/pnas.1913714116, 2019.

Liu, J. T., Kao, S. J., Huh, C. A., and Hung, C. C.: Gravity flows associated with flood events and carbon burial: Taiwan as instructional source area, Ann Rev Mar Sci, 5, 47-68, 10.1146/annurev-marine-121211-172307, 2013.

Liu, Z., Zhao, Y., Colin, C., Stattegger, K., Wiesner, M. G., Huh, C.-A., Zhang, Y., Li, X., Sompongchaiyakul, P., You, C.-F., Huang, C.-Y., Liu, J. T., Siringan, F. P., Le, K. P., Sathiamurthy, E., Hantoro, W. S., Liu, J., Tuo, S., Zhao, S., Zhou, S., He, Z., Wang, Y., Bunsomboonsakul, S., and Li, Y.: Source-to-sink transport processes of fluvial sediments in the South China Sea, Earth-Science Reviews, 153, 238-273, 10.1016/j.earscirev.2015.08.005, 2016.

McArthur, A. D., Kneller, B. C., Wakefield, M. I., Souza, P. A., and Kuchle, J.: Palynofacies classification of the depositional elements of confined turbidite systems: Examples from the Gres d'Annot, SE France, Marine and Petroleum Geology, 77, 1254-1273, 10.1016/j.marpetgeo.2016.08.020, 2016.

McGlue, M. M., Smith, P. H., Zani, H., Silva, A., Carrapa, B., Cohen, A. S., and Pepper, M. B.: An Integrated Sedimentary Systems Analysis of the Rio Bermejo (Argentina): Megafan Character in the Overfilled Southern Chaco Foreland Basin, J Sediment Res, 86, 1359-1377, 10.2110/jsr.2016.82, 2016.

Nichols, G. J., Cripps, J. A., Collinson, M. E., and Scott, A. C.: Experiments in waterlogging and sedimentology of charcoal: results and implications, Palaeogeography, Palaeoclimatology, Palaeoecology, 164, 43–56, https://doi.org/10.1016/S0031-0182(00)00174-7, 2000.

Nieto-Moreno, V., Rohrmann, A., van der Meer, M. T. J., Sinninghe Damsté, J. S., Sachse, D., Tofelde, S., Niedermeyer, E. M., Strecker, M. R., and Mulch, A.: Elevation-dependent changes in n -alkane δ D and soil GDGTs across the South Central Andes, Earth and Planetary Science Letters, 453, 234-242, 10.1016/j.epsl.2016.07.049, 2016.

https://doi.org/10.5194/egusphere-2023-2485
Preprint. Discussion started: 13 November 2023


Parsons, D. R., Jackson, P. R., Czuba, J. A., Engel, F. L., Rhoads, B. L., Oberg, K. A., Best, J. L., Mueller, D. S., Johnson, K. K., and Riley, J. D.: Velocity Mapping Toolbox (VMT): a processing and visualization suite for moving-vessel ADCP measurements, Earth Surface Processes and Landforms, 38, 1244-1260, 10.1002/esp.3367, 2013.

Ponton, C., West, A. J., Feakins, S. J., and Galy, V.: Leaf wax biomarkers in transit record river catchment composition, Geophysical Research Letters, 41, 6420-6427, 10.1002/2014gl061328, 2014.

Powell, R. L., Zoo, E.-H., and Still, C. J.: Vegetation and soil carbon-13 isoscapes for South America integrating remote sensing and ecosystem isotope measurements, Ecosphere, 3(11).109, https://doi.org/10.1890/ES12-00162.1, 2012.

Rach, O., Hadeen, X., and Sachse, D.: An automated solid phase extraction procedure for lipid biomarker purification and stable isotope analysis, Organic Geochemistry, 142, 10.1016/j.orggeochem.2020.103995, 2020.

Reid, I., Laronne, J. B., and Powell, D. M.: Flash-flood and bedload dynamics of desert gravel-bed streams, Hydrological Processes, 12, 543-557, https://doi.org/10.1002/(SICI)1099-1085(19980330)12:4<543::AID-HYP593>3.0.CO;2-C, 1998.

Repasch, M.: Lithospheric flexure controls on geomorphology, hydrology, and river chemistry in the Andean foreland basin, 2023.

Repasch, M., Scheingross, J. S., Hovius, N., Vieth-Hillebrand, A., Mueller, C. W., Höschen, C., Szupiany, R. N., and Sachse, D.: River Organic Carbon Fluxes Modulated by Hydrodynamic Sorting of Particulate Organic Matter, Geophysical Research Letters, 49, 10.1029/2021gl096343, 2022.

Repasch, M., Wittmann, H., Scheingross, J. S., Sachse, D., Szupiany, R., Orfeo, O., Fuchs, M., and Hovius, N.: Sediment Transit Time and Floodplain Storage Dynamics in Alluvial Rivers Revealed by Meteoric10Be, Journal of Geophysical Research: Earth Surface, 125, 10.1029/2019jf005419, 2020.

Rickenmann, D.: Variability of Bed Load Transport During Six Summers of Continuous Measurements in Two Austrian Mountain Streams (Fischbach and Ruetz), Water Resources Research, 54, 107-131, https://doi.org/10.1002/2017WR021376, 2018.

Rohrmann, A., Strecker, M. R., Bookhagen, B., Mulch, A., Sachse, D., Pingel, H., Alonso, R. N., Schildgen, T. F., and Montero, C.: Can stable isotopes ride out the storms? The role of convection for water isotopes in models, records, and paleoaltimetry studies in the central Andes, Earth and Planetary Science Letters, 407, 187-195, 10.1016/j.epsl.2014.09.021, 2014.

Ruiz-Villanueva, V., Mazzorana, B., Bladé, E., Bürkli, L., Iribarren-Anacona, P., Mao, L., Nakamura, F., Ravazzolo, D., Rickenmann, D., Sanz-Ramos, M., Stoffel, M., and Wohl, E.: Characterization of wood-laden flows in rivers, Earth Surface Processes and Landforms, 44, 1694-1709, 10.1002/esp.4603, 2019.

Sachse, D., Radke, J., and Gleixner, G.: Hydrogen isotope ratios of recent lacustrine sedimentary n-alkanes record modern climate variability, Geochimica et Cosmochimica Acta, 68, 4877-4889, 10.1016/j.gca.2004.06.004, 2004.

Sachse, D., Billault, I., Bowen, G. J., Chikaraishi, Y., Dawson, T. E., Feakins, S. J., Freeman, K. H., Magill, C. R., McInerney, F. A., Meer, M. T. J. v. d., Polissar, P., Robins, R. J., Sachs, J. P., Schmidt, H.-L., Sessions, A. L., White, J. W. C., West, J. B., and Kahmen, A.: Molecular Paleohydrology: Interpreting the Hydrogen-Isotopic Composition of Lipid Biomarkers from

https://doi.org/10.5194/egusphere-2023-2485
Preprint. Discussion started: 13 November 2023


Photosynthesizing Organisms, Annual Review of Earth and Planetary Sciences, 40, 221-249, 10.1146/annurev-earth-042711-105535, 2012a.

Sachse, D., Billault, I., Bowen, G. J., Chikaraishi, Y., Dawson, T. E., Feakins, S. J., Freeman, K. H., Magill, C. R., McInerney, F. A., van der Meer, M. T. J., Polissar, P., Robins, R. J., Sachs, J. P., Schmidt, H.-L., Sessions, A. L., White, J. W. C., West, J. B., and Kahmen, A.: Molecular Paleohydrology: Interpreting the Hydrogen-Isotopic Composition of Lipid Biomarkers from Photosynthesizing Organisms, Annual Review of Earth and Planetary Sciences, 40, 221-249, 10.1146/annurev-earth-042711-105535, 2012b.

Sambrook Smith, G. H., Best, J. L., Leroy, J. Z., Orfeo, O., and Baas, J.: The alluvial architecture of a suspended sediment dominated meandering river: the Río Bermejo, Argentina, Sedimentology, 63, 1187-1208, 10.1111/sed.12256, 2016.

Schefuss, E., Schouten, S., and Schneider, R. R.: Climatic controls on central African hydrology during the past 20,000 years, Nature, 437, 1003-1006, 10.1038/nature03945, 2005.

Scheingross, J. S., Hovius, N., Dellinger, M., Hilton, R. G., Repasch, M., Sachse, D., Gröcke, D. R., Vieth-Hillebrand, A., and Turowski, J. M.: Preservation of organic carbon during active fluvial transport and particle abrasion, Geology, 47, 958-962, 10.1130/g46442.1, 2019.

Scheingross, J. S., Repasch, M. N., Hovius, N., Sachse, D., Lupker, M., Fuchs, M., Halevy, I., Gröcke, D. R., Golombek, N. Y., Haghipour, N., Eglinton, T. I., Orfeo, O., and Schleicher, A. M.: The fate of fluvially-deposited organic carbon during transient floodplain storage, Earth and Planetary Science Letters, 561, 10.1016/j.epsl.2021.116822, 2021.

Schlünz, B. and Schneider, R. R.: Transport of terrestrial organic carbon to the oceans by rivers: re-estimating flux- and burial rates, International Journal of Earth Sciences, 88, 599-606, 10.1007/s005310050290, 2000.

Schwab, M. S., Hilton, R. G., Haghipour, N., Baronas, J. J., and Eglinton, T. I.: Vegetal Undercurrents—Obscured Riverine Dynamics of Plant Debris, Journal of Geophysical Research: Biogeosciences, 127, 10.1029/2021jg006726, 2022.

Selva, E. C., Couto, E. G., Johnson, M. S., and Lehmann, J.: Litterfall production and fluvial export in headwater catchments of the southern Amazon, Journal of Tropical Ecology, 23, 329-335, 10.1017/s0266467406003956, 2007.

Seo, J. I., Nakamura, F., Nakano, D., Ichiyanagi, H., and Chun, K. W.: Factors controlling the fluvial export of large woody debris, and its contribution to organic carbon budgets at watershed scales, Water Resources Research, 44, 10.1029/2007wr006453, 2008.

Silva, L. C. R., Giorgis, M. A., Anand, M., Enrico, L., Pérez-Harguindeguy, N., Falczuk, V., Tieszen, L. L., and Cabido, M.: Evidence of shift in C4 species range in central Argentina during the late Holocene, Plant and Soil, 349, 261-279, 10.1007/s11104-011-0868-x, 2011.

Smith, J. A., Mazumder, D., Suthers, I. M., Taylor, M. D., and Bowen, G.: To fit or not to fit: evaluating stable isotope mixing models using simulated mixing polygons, Methods in Ecology and Evolution, 4, 612-618, 10.1111/2041-210x.12048, 2013a.

Smith, J. C., Galy, A., Hovius, N., Tye, A. M., Turowski, J. M., and Schleppi, P.: Runoff-driven export of particulate organic carbon from soil in temperate forested uplands, Earth and Planetary Science Letters, 365, 198-208, 10.1016/j.epsl.2013.01.027, 2013b.

https://doi.org/10.5194/egusphere-2023-2485
Preprint. Discussion started: 13 November 2023


Spacesystems, N. M. A. J. and Team, U. S. J. A. S.: ASTER Global Digital Elevation Model NetCDF V003, NASA EOSDIS Land Processes DAAC, https://doi.org/10.5067/MEaSUREs/NASADEM/NASADEM_NC.001, 2019.

Sparkes, R. B., Lin, I.-T., Hovius, N., Galy, A., Liu, J. T., Xu, X., and Yang, R.: Redistribution of multi-phase particulate organic carbon in a marine shelf and canyon system during an exceptional river flood: Effects of Typhoon Morakot on the Gaoping River–Canyon system, Marine Geology, 363, 191-201, 10.1016/j.margeo.2015.02.013, 2015.

Stallard, R. F.: Terrestrial sedimentation and the carbon cycle: Coupling weathering and erosion to carbon burial, Global Biogeochemical Cycles, 12, 231-257, 10.1029/98gb00741, 1998.

Stewart, M. K. and Taylor, C. B.: Environmental isotopes in New Zealand hydrology ; 1 Introduction The role of oxygen-18, deuterium, and tritium in hydrology, New Zealand journal of science, 295-311, 1981.

Thomas, C. L., Jansen, B., van Loon, E. E., and Wiesenberg, G. L. B.: Transformation of n-alkanes from plant to soil: a review, Soil, 7, 785-809, 10.5194/soil-7-785-2021, 2021.

Turowski, J. M., Hilton, R. G., and Sparkes, R.: Decadal carbon discharge by a mountain stream is dominated by coarse organic matter, Geology, 44, 27-30, 10.1130/g37192.1, 2016.

Turowski, J. M., Badoux, A., Bunte, K., Rickli, C., Federspiel, N., and Jochner, M.: The mass distribution of coarse particulate organic matter exported from an Alpine headwater stream, Earth Surface Dynamics, 1, 1-11, 10.5194/esurf-1-1-2013, 2013.

Tyson, R. V. and Follows, B.: Palynofacies prediction of distance from sediment source- A case study from the Upper Cretaceous of the Pyrenees, Geology, 28, 569–571, 2000.

Walker, C. D. and Richardson, S. B.: The use of stable isotopes of water in characterising the source of water in vegetation, Chemical Geology: Isotope Geoscience section, 94, 145-158, https://doi.org/10.1016/0168-9622(91)90007-J, 1991.

West, A. J., Lin, C. W., Lin, T. C., Hilton, R. G., Liu, S. H., Chang, C. T., Lin, K. C., Galy, A., Sparkes, R. B., and Hovius, N.: Mobilization and transport of coarse woody debris to the oceans triggered by an extreme tropical storm, Limnology and Oceanography, 56, 77-85, 10.4319/lo.2011.56.1.0077, 2011.

Wohl, E., Ogden, F. L., and Goode, J.: Episodic wood loading in a mountainous neotropical watershed, Geomorphology, 111, 149-159, 10.1016/j.geomorph.2009.04.013, 2009.

Wohl, E., Kramer, N., Ruiz-Villanueva, V., Scott, D. N., Comiti, F., Gurnell, A. M., Piegay, H., Lininger, K. B., Jaeger, K. L., Walters, D. M., and Fausch, K. D.: The Natural Wood Regime in Rivers, BioScience, 69, 259-273, 10.1093/biosci/biz013, 2019.

Yager, E. M., Turowski, J. M., Rickenmann, D., and McArdell, B. W.: Sediment supply, grain protrusion, and bedload transport in mountain streams, Geophysical Research Letters, 39, n/a-n/a, 10.1029/2012gl051654, 2012.

Literature

https://doi.org/10.5194/egusphere-2023-2485
Preprint. Discussion started: 13 November 2023


Crameri, F.: Scientific colour maps (7.0.0), https://doi.org/10.5281/zenodo.4491293, 2021.